1972 ANNUAL REPORT ON THE INVESTIGATION OF CRITICAL BURNING OF FUEL DROPLETS

by

C. B. Allison, G. S. Canada, and G. M. Faeth

Mechanical Engineering Department
The Pennsylvania State University
University Park, Pennsylvania

prepared for

Table of Contents

1972 ANNUAL REPORT ON THE INVESTIGATION OF
CRITICAL PRESSURE BURNING OF FUEL DROPLETS

Summary

This report discusses activities under NASA Contract NGR 39-009-077 for the period January 1, 1972, through December 31, 1972. During this period the investigation was divided into four phases, the results for each phase may be summarized as follows:

1. Droplet Combustion at High Pressures. Combustion of methanol, ethanol, propanol-1, n-pentane, n-heptane and n-decane from porous spheres was observed in air under natural convection conditions at pressures up to 100 atm. The pressure levels of the tests were high enough so that near critical combustion was observed for methanol and ethanol. Measurements were made of the burning rate and liquid surface temperatures of the fuels. Due to the high pressures, the phase equilibrium models of the analysis included both low and high pressure versions, the latter allowing for real gas effects and the solubility of the combustion product gases in the liquid phase. The burning rate predictions of the various theories were similar and in fair agreement with the data. The experiments indicated the approach of critical burning conditions for methanol and ethanol at pressures on the order of 80-100 atm, which was in good agreement with the predictions of both the low and high pressure analysis for these fuels. Critical burning conditions could not be approached for the remaining fuels due to the formation of soot deposits on the sphere at pressures in the range 30-60 atm.

2. High Pressure Droplet Burning in Combustion Gases. An experimental apparatus was constructed to allow measurements of the steady combustion of liquid fuels from porous spheres in an environment that simulates combustion chamber conditions. The apparatus employs a burner contained within a pressure vessel to allow operation at various oxygen concentrations, gas velocities and pressures ranging up to 35 atm. During the coming report period, testing and analysis will be completed for the same range of fuel types considered in the natural convection tests.

3. Liquid Strand Combustion. Burning rates and liquid surface temperatures were measured for burning liquid strands of hydrazine over the pressure range 7-600 psia. At pressures greater than 1 atm, the burning rate was found to increase linearly with pressure. The addition of water to the hydrazine resulted in a marked reduction in the burning rate. Liquid surface temperatures were found to be in good agreement with predictions based on a low pressure phase equilibrium model for pressures up to 300 psia.

4. <u>Oscillatory Combustion</u>. An experimental apparatus has been con-
structed to allow measurement of the response of a burning liquid
hydrazine strand to imposed pressure oscillations. Due to the ability
of hydrazine to burn at very slow rates as a strand, this apparatus
is capable of observing the response at frequencies comparable to
the critical frequency of liquid phase transient effects, providing
a good test of the oscillatory theory. Equations are developed for
the oscillatory theory of the response through first order in the
amplitude of the pressure oscillations. During the coming report
period experimental results will be completed and compared with
theoretical computations.

I. Introduction

The objective of this study is to investigate the combustion and evaporation of liquid fuels at high pressures. Particular emphasis is placed on conditions where the liquid surface approaches the thermodynamic critical point during combustion. The influence of transient effects on a burning liquid fuel is also being investigated through both analysis and measurements of the response of liquid monopropellant combustion to imposed pressure oscillations. This report gives a summary of progress on the investigation for the period January 1, 1972, to December 31, 1972.

Work during this report period was divided into four phases as follows: (1) Droplet Combustion at High Pressures, which considers both measurement and analysis of the porous sphere burning rate of liquids in a natural convection environment at elevated pressure. Work in this area was concluded during the report period. (2) High Pressure Droplet Burning in Combustion Gases, which involves steady burning and evaporation of liquids from porous spheres in a high pressure environment that simulates actual combustion chamber conditions. Work in this area is currently in progress. (3) Liquid Strand Combustion, which considers the burning rate, the state of the liquid surface and the liquid phase temperature distribution of a burning liquid monopropellant column over a range of pressures. Work in this area was concluded during the report period. (4) Oscillatory Combustion, which is a theoretical and experimental investigation of the response of a burning liquid monopropellant to pressure oscillations. Work in this area is currently in progress.

In the following sections, the activity in each phase is summarized for the report period. Wherever possible, the details of the work are presented by reference to past publications and only material not previously reported is given extended coverage. Reference 1, 15, and 25 comprise other publications resulting from work done on this project which have appeared during the period of this report.

II. Droplet Combustion at High Pressures

Introduction:

The objective of this part of the investigation was to study high pressure droplet combustion for a variety of fuels. This included the experimental determination of burning rates and liquid surface temperatures. The experimental results were compared with droplet combustion theories which both neglected and considered real gas effects. The fuels used in the tests consisted of methanol, ethanol, propanol-1, n-pentane, n-heptane, and n-decane. The pressure range varied from 1 to 51 atmospheres for the hydrocarbon fuels and from 1 to 78 atmospheres for the alcohols. Porous alundum spheres were used to simulate the fuel droplets. The sphere sizes included 0.63 cm. 0.95 cm and 1.9 cm diameter spheres.

In addition to the determination of burning rates and liquid surface temperatures, a series of dark field photographs were taken. Methanol and

ethanol were the fuels used in these tests. The sphere sizes employed were
0.63 cm, 0.95 cm and 1.9 cm, in the pressure range from 1 to 35 atmospheres.
The findings of this portion of the investigation are summarized in greater
detail in Reference 1.

Experimental Apparatus:

A sketch of the overall system is shown in Figure 1. The high-pressure
combustion apparatus consists of a thick-walled steel cylindrical vessel
66 cm. long with an inside diameter of 13 cm. The chamber is fitted with
windows to allow observation of the combustion process.

The porous spheres used in the combustion tests are made of alundum.
The fuel is fed to the center of the sphere through a stainless steel
water cooled tube. The outside diameter of the coolant tube was 0.20 cm
for the 0.64 cm diameter sphere and 0.32 cm for the larger spheres. The
fuel flow rate was controlled by a variable displacement diaphragm pump
and measured with a system of graduated burets at the pump inlet. The
steady burning rate was determined as the flow rate where the surface of
the sphere is fully wet but not dripping.

Air for the combustion process is supplied by a 3000 psia compressor
which is accurately controlled by a critical flow jeweled orifice system
of the type described by Anderson and Friedman (2). The hot exhaust gases
leaving the reactor are cooled with water in a concentric tube heat ex-
changer. Water condensate is collected in a trap which is periodically
blown off to a drain.

Liquid surface temperatures were measured using two 0.0076 cm diameter
chromel-alumel thermocouples. All liquid surface temperature determinations
were made using the 0.95 cm diameter sphere. The thermocouples were cemented
flush with the surface and located 60 degrees apart along the periphery of
the sphere. A constant gas composition was maintained around the sphere by
admitting air through a manifold at the bottom of test chamber. The drift
velocity of the flow of air past the sphere was sufficiently low so that
natural convection was the predominant convection effect.

The dark field photographs were taken using a 4 in. x 5 in. Super Graflex
camera fitted with a 135 mm Optar lens. The film used was Polaroid type 57
land film with an ASA rating of 3000.

Theoretical Analysis:

The present theory is similar in many respects to that of References 3 and
4 for high pressure combustion. The major point of difference involves the
different boundary conditions at the liquid surface for the present porous
sphere combustion case as opposed to steady droplet combustion, and a
correction to the burning rate for natural convection effects.

The theory is divided into a gas phase model of the combustion process
and a phase equilibrium model for conditions at the liquid surface. In the
gas phase model, the effect of convection is treated by the use of the
multiplicative correction of the burning rate predicted in the absence of
convection similar to that employed in References 5 and 6. Therefore, the
basic analysis assumes spherical symmetry and neglects convection effects.
The process is assumed to be steady and the total pressure is taken to be

uniform throughout the system. Both dissociation and radiation are neglected and the reaction is assumed to be confined to an infinitely thin flame surface where fuel and oxidizer combine in stoichiometric proportions.

Only concentration diffusion is considered in the gas phase and the influence of compressibility on transport properties is neglected. In addition, the concentration dependence of the thermal conductivity is neglected and the binary diffusivities of all species are taken to be the same, although different values of each of these properties can be employed inside and outside the flame. The common unity Lewis number assumption was not employed in the analysis since earlier studies (3, 4) have shown that the value of the Lewis number has a strong influence on conditions at the liquid surface.

A sketch of the model of the burning droplet is shown in Figure 2. In the present experiment, the liquid fuel was pumped from a storage vessel at atmospheric pressure to the center of the sphere. Therefore, due to the low solubility of gases in the test fuels at low pressures, it is appropriate to assume that the liquid entering the sphere has a neglibible dissolved gas concentration. Under this assumption, the liquid phase flux of dissolved gas is zero and the fuel is the only component with a finite molar flux inside the flame surface.

The specific heat of each species was assumed to be a linear function of temperature*

$$C_{pi} = a_i + b_i T. \tag{1}$$

where a_i and b_i are fixed constants for species i.

The thermal conductivity was also assumed to be proportional to temperature in the regions inside and outside the flame

$$\lambda = \lambda_s (T/T_s). \tag{2}$$

The quantity

$$\chi = \lambda/(cD) \tag{3}$$

is only a weak function of temperature and composition and was assumed to be a constant inside and outside the flame.

With due allowance for the fact that the fuel mole flux fraction is unity in the region inside the flame, the details of the gas phase analysis are very similar to that presented in References 3 and 4. The specific results obtained in the present case are given in Reference 1. In addition to this variable property - variable specific heat analysis, calculations were also performed for variable property - constant specific heat and constant property models.

---

*See the nomenclature at the end of this section for the meaning of symbols.

The semi-empirical correction, for the effect of natural convection on the burning rate, [5,6] was based on the natural convection heat transfer correlation determined by Yuge.[7] In addition, the Grashoff number for burning spheres suggested by Spalding [8] was employed in the correlation. The specific equation used in the calculations is as follows

$$\frac{\dot{n}}{\dot{n}_o} = 1 + 0.221 \, Pr^{1/3} (d^3 g/\nu^2)^{1/4} \tag{4}$$

In order to avoid ambiguity, the properties used in this correlation were taken at the ambient conditions of the burning sphere.

Three models were employed for computing phase equilibrium at the liquid surface. The simplest model (low pressure theory) neglected the solubility of the product gases in the liquid phase and other high pressure corrections. The fuel mole fraction at the liquid surface was taken to be the vapor pressure of the pure fuel, at the surface temperature, divided by the total pressure. The total enthalpy rise of vaporization was determined by summing the compressed liquid enthalpy change at T_o (the fuel inlet temperature), the heat of vaporization at T_o, the ideal gas enthalpy rise between T_o and T_s (the surface temperature) and the enthalpy deviations between saturated vapor and the ideal gas states at T_o and T_s. In this case, the ideal gas enthalpy rise was computed by integrating actual specific heat correlations between T_o and T_s, as opposed to the linearized specific heat correlation (Equation 1) employed in the gas phase analysis. The enthalpy deviations were obtained from the tables of Lyderson, et al, presented in Reference 9.

The high-pressure theories considered solubility and other high-pressure effects through the use of a modified Redlick-Kwong equation of state with mixing rules given by Prausnitz and Chueh.[10] For combustion in air, the major gaseous species at the liquid surface are fuel vapor, nitrogen, carbon dioxide and water vapor. Since nitrogen predominates the non-fuel gases in this system, a simplified version of the high pressure theory assumed that this system could be represented by a binary mixture of fuel and nitrogen. The more complete version of the high pressure theory considered the complete quaternary system; fuel, nitrogen, carbon dioxide and water.

The details of the formulation of the high pressure phase equilibrium model are given in Reference 4. The dimensionless constants required by the Redlick-Kwong equation of state were obtained by setting the first and second isothermal derivatives of pressure, with respect to volume, equal to zero at the critical point. The binary interaction parameters, k_{ij}, required by the theory are listed in Reference 3 for the paraffins and the combustion product gases. For the alcohols, the k_{ij} values were taken to be the same as that of the hydrocarbon homomorph of fuel. These values are listed in Reference 1. For the high pressure theories, the enthalpy deviations required in the calculation of the total heat of vaporization of the fuel were computed directly from the Redlick-Kwong equation of state. The remaining terms comprising the enthalpy rise of vaporization were computed in the same manner as in the low pressure theory calculations.

The sources of property data and correlations were the same as in earlier studies. [3,4,5] The particular values employed in the present calculations are given in Reference 1 along with a description of the calculation procedure.

Results:

Sooting was a serious problem with all of the hydrocarbon fuels tested. Methanol did not present this problem and only at very high pressures (around 1100 psia) did ethanol begin sooting. Propanol-1, on the other hand, exhibited sooting problems at much lower pressures. The upper limit due to sooting for n-decane was 32 atmospheres.

The tests using ethanol as a fuel were terminated around 72 atmospheres since it was impossible to determine the nature of the sphere surface at pressures in excess of this. Methanol presented this problem also but at slightly higher pressures. In both cases vapor jets were observed rather than liquid drops. Critical combustion could account for this effect although the pressure at which this condition occurred could not be precisely determined.

The experimental burning rates for the alcohols are shown in Figure 3. The burning rate data for the hydrocarbon fuels (Figure 4) were terminated at high pressure due to the formation of soot. When this occurred, carbon spots would form and grow on the surface of the sphere. As can be seen from Figures 3 and 4, the theory gives a reasonably good indication of the rate of increase of the burning rate with increasing pressure.

The effect of varying sphere size is examined for methanol, n-heptane and n-decane in Figure 5. For this plot, the dimensionless burning rate, normalized by the convection correction is employed for the ordinate so that the data for various sphere sizes should fall on a single curve. It is seen that the normalized burning rate (which corresponds to no-convection burning rate of the theory) is almost a constant up to the critical burning condition for the present porous sphere experiments. This indicates that the burning rate increase with increasing pressure in Figure 2 and 3 is largely due to convection effects. The present experimental results represent a reasonably good test of the burning rate correction for natural convection, since the Grashoff number based on the Spalding definition (8) varies in range $10^4 - 10^8$.

Liquid surface temperatures for the six fuels are illustrated in Figures 6 and 7. The boiling point curves and the surface temperature predictions of both the low-pressure and quartenary high-pressure theories are shown on the figures along with the data. The data for ethanol and propanol-1 (Figure 6) agrees reasonably well with the high pressure theory at the high pressures. However, the low pressure theory gives the best estimation of data over the entire test range for methanol. The poorer high-pressure theoretical results for methanol could be attributed to the large quantities of water vapor in the combustion products of this fuel. Water is difficult to model precisely in the high-pressure phase equilibrium analysis, and materials with high water vapor concentrations have generally shown poorer agreement with the high-pressure theory in the past (15).

The data for the paraffins (Figure 7) could not be extended to sufficiently high pressures to provide an adequate test of high pressure theory due to the formation of soot. However, the low pressure theory appears to be adequate for these fuels over the available experimental range.

The simplified binary model gave essentially the same results with regard to burning rates and liquid surface temperature as the quaternary

phase equilibrium model. However, in contrast to high pressure droplet combustion where the binary model also gave a good estimation of critical burning conditions there were significant differences between the critical porous sphere combustion pressures predicted by the two high-pressure theories. The critical combustion conditions for all three theories are compared with pure fuel critical properties in Table I. In agreement with the experimental findings, both the low and high pressure quaternary theories predict critical burning pressures on the order of 100 atm for methanol and ethanol. The theoretical indication that ethanol should experience critical burning at pressures somewhat below methanol is also in qualitative agreement with the fact that experimental difficulties in determining burning rates were encountered at somewhat lower pressure for ethanol, c.f. Figure 3.

The theoretical results were obtained with the variable property-variable specific heat gas phase analysis, using the properties listed in Reference 1. The use of the variable property-constant specific heat and constant property gas phase analysis gave essentially the same results, when the respective constant properties in each of these cases was evalutaed at average conditions in each region.

Summary and Conclusions:

The low and high pressure theories gave essentially the same prediction of burning rates at high pressures. The greatest differences between the theories were encountered in the prediction of liquid surface temperatures and critical burning conditions. The quaternary high pressure theory gave the best agreement with experimental results for ethanol and propanol-1, whereas the low pressure theory gave the best predictions for methanol.

The experiments indicated that the methanol and ethanol were approaching critical combustion conditions at pressures on the order of 80-100 atm. Both the low pressure and high pressure quaternary theories predicted critical burning in reasonable agreement with these results. Critical burning conditions could not be approached for the remaining fuels due to the formation of soot deposits on the sphere over the pressure range of 30-60 atm.

The use of variable property-variable specific heat, variable property-constant specific heat and constant property gas phase analyses gave essentially the same results as long as the respective constant properties were evaluated at average conditions inside and outside the flame. Parametric property variations caused variations in the computed results similar to those encountered in earlier high pressure combustion studies (3, 4, 15). For porous spheres, the binary high-pressure theory gave a poorer approximation of the quaternary high-pressure theory, then was the case for high pressure droplet combustion (3).

Work has been completed on this phase of the investigation for droplet combustion in a cold gas environment.

Nomenclature, Section II:

a_i, b_i	Specific heat parameters, Equation (1)
c	Concentration
C_{pi}	Specific heat of species i
d	Droplet diameter
D	Diffusion coefficient
g	Acceleration of gravity
k_{ij}	Binary interaction parameters
K, K_o	Burning rate constant with and without convection
$\dot{n}$, $\dot{n}_o$	Total molar flow rate with and without convection
P_r	Prandtl number
R_e	Reynolds number
T	Temperature
λ	Thermal conductivity
ν	Kinematic viscosity
χ	Parameter, Equation (3)

Subscripts

o	Initial conditions
s	Liquid surface

III. High Pressure Droplet Burning in Combustion Gases

Introduction:

The objectives of this portion of the investigation include the determination of high pressure droplet burning and evaporation rates and liquid surface temperatures in a combustion chamber environment. The range of fuels to be considered will be the same as the high pres-

sure natural convection tests. The oxygen concentration in the combustion gases will be varied and will include the limiting case of high temperature evaporation without combustion. In addition, the experiments will include various flow velocities past the test droplet and various pressure levels to provide an evaluation of both forced convection and high pressure effects. The experimental results will also be compared with high pressure combustion theories.

In order to simulate a combustion chamber environment for the porous fuel spheres, a burner is used to produce the hot combustion gases. The burner provides an added advantage in that the composition of the gases can be accurately controlled. The burner design is of the swirl-stabilized diffusion type. Other major advantages of a burner of this type include a relatively simple design, stable operation over a wide range of flow conditions, and the elimination of flashback. In earlier tests with premixed flat flame burners, flashback posed serious problems.

The burner used in the current tests employs a flame supplied with a mixture of carbon monoxide and air. Carbon monoxide was chosen for a fuel since it is quite stable, has a reduced tendency to smoke and minimizes the problem of water condensation within the apparatus.

Experimental Apparatus:

A sketch of the high pressure combustion rig with the burner is shown in Figure 8. The basic reactor vessel is similar to the one that was used for the cold gas droplet burning tests. There are, however, several modifications that were not present on the former apparatus. These include an internal stainless steel cooling coil to keep the apparatus' walls cool and to reduce radiation from the walls to the fuel droplet. Observation of the combustion process is made through quartz windows located at the test section. The fuel delivery and measuring system is the same as that described for the cold gas tests. There are four major burner components. These include the stainless steel burner base containing the fuel and oxidizer injectors, a spark-ignition system, a ceramic flow straightener, and a steel outer jacket.

The internal diameter of the burner test section is 5.08 cm. The burner wall consists of alundum tubing and alumina firebrick. Fuel is admitted through an injector located in the center of the burner base and the oxidizer is admitted through two tangential injectors located along the inner wall of the burner. A flow straightener is located in the burner passage to insure that the velocity and temperature profiles of the hot gases will be uniform when the test section is reached. All gas flows are metered by critical flow orifices. To determine gas temperature, a system of platinum-platinum rhodium fine wire thermocouples is located in the test section. To reduce oxidation and catalytic effects the thermocouples are coated with silicone using a procedure outlined by Fristrom and Westenberg (11). As a check of the gas temperature measurements, the composition and temperature of the gas at the droplet location are also computed from thermochemical calculations. For these calculations, allowance is made for dissociation and heat loss through the burner walls.

Theoretical Analysis:

The theoretical results and analysis of the high pressure theory will be employed in this phase of the investigation. As was pointed out in the discussion of results in the portion of the report dealing with high pressure droplet combustion, the high pressure model gave adequate agreement with the experimental results for the range of fuels tested. Therefore, this model will be used but with one major exception. The convection correction that accounts for the influence of the flow of burning gas past the test droplet is different than that used for the cold gas tests (which were essentially free convection tests).

The specific correlation for the present tests follows a form which was previously employed in Reference 5.

$$K/K_o = 1 + 0.278 \, R_e^{1/2} \, Pr^{1/3} \, (1 + 1.237/RePr^{4/3})^{-1/2}$$

where K and K_o are the burning rate constants with and without convection present.

This expression has the advantage of asymptotically approaching the mathematically rigorous results of Fendell et.al (12) for small Peclet numbers as well as agreeing with the data of Frössling (13), Yuge (7) and Allender (14) for 10<Re<800.

Results:

The experimental apparatus for high pressure droplet burning rate measurements in a combustion gas environment has been assembled. In preliminary tests, the swirl stabilized burner has been operated for extended periods of time at elevated pressures. During these tests, no difficulties were encountered with regard to overheating the structure of the apparatus. The burner flame was found to be quite stable for operation at various gas pressures, mixture ratios and velocities.

Testing with porous spheres is currently in progress. Complete combustion testing as well as analysis of the results will be completed during the coming report period. The pressure range of these tests will extend to pressures on the order of 35 atm, which is sufficient to reach conditions where critical point phenomena become important.

Summary and Conclusions:

An apparatus has been constructed to allow measurements of steady evaporation and combustion of liquid fuels in an environment which simulates combustion chamber conditions. During the coming report period, testing will be completed for a range of fuels, oxygen concentrations, gas velocities and pressures; these results will be compared with analytical results which allow for the effect of high pressure phenomena, ambient gas solubility, etc.

IV. <u>Liquid Strand Combustion</u>

Introduction:

The purpose of this portion of the investigation is to study the temperature distribution and dissolved gas concentration in a burning liquid monopropellant strand at high pressures. Earlier work concentrated on the nitrate ester fuels (15). The study described here is concerned with hydrazine.

During this report period, burning rate measurements of liquid strands of hydrazine were extended from previous by reported results (16) to include the effect of tube diameter and liquid phase concentration. Also, liquid surface temperature measurements were obtained over a pressure range of 7 to 300 psia. These temperature measurements were compared to the infinite activation energy theoretical model of Faeth (15) and also to predictions based on the familiar unity Lewis number assumption.

Experimental Apparatus:

Since the strand burner apparatus has been described in detail in Reference 16, only a brief description of its operation will be given here. With the strand burner technique, liquid fuel is placed in a glass tube contained within a windowed pressure vessel. The vessel is pressurized with nitrogen to the desired test pressure. Following ignition with a heater coil, the fuel burns down the tube. As the combustion zone propagates past the window in the chamber, the rate of regression of the liquid column as well as the position of the thermocouple with respect to the liquid surface is determined from motion picture shadowgraphs. The temperature registered by the thermocouple is recorded on an oscillograph with a flat frequency response to 2000 Hz.

The thermocouples were constructed of 0.0003 inch O.D. platinum - platinum 10% rhodium butt welded wire as described in Reference 11. Since the pressure levels and burning rates for the hydrazine tests were considerably lower than the conditions encountered in earlier testing (15, 16), the cold reference junction of the thermocouple was relocated outside the apparatus in order to obtain a steady reference temperature. Otherwise, the apparatus used was as described in Reference 15.

Theoretical Analysis:

Since the process is steady, the gas and liquid phases are considered separately. However, phase equilibrium requires the two solutions to match at the liquid surface.

Two gas phase models were used. The first model has been described in detail by Faeth (15). This model assumes an infinitely thin decomposition flame (infinite activation energy) and the gas phase specific heat and thermal conductivity are assumed to vary linearly with temperature. In the second model, the unity Lewis number assumption is used and the gas phase specific heat is assumed to be constant but thermal conductivity is assumed to vary linearly with temperature. For both models the ratio of gas phase thermal conductivity to the concentration of fuel times the diffusion coefficient is assumed to be constant. The flame temperature, assuming an adiabatic deflagration wave, and product gas concentrations were determined from thermochemical calculations allowing for all relevant dissociation

reactions. Data for these calculations were obtained from the JANNAF Tables (17). All other properties were computed as in Reference 1.

Two models of phase equilibrium at the liquid surface have previously been used (15). The low pressure model neglects high pressure corrections and ambient gas solubility in the liquid phase. The mole fraction of fuel at the liquid surface is taken to be the ratio of vapor pressure of fuel at the liquid surface temperature to the total pressure. The more complete high pressure model accounts for high pressure effects and the solubility of the combustion products in the liquid phase. Since the pressure levels for the hydrazine tests were much less than the critical pressure, only the low pressure phase equilibrium model has been applied to the hydrazine data.

With the low pressure phase equilibrium model, one relation between the liquid surface temperature and fuel mole fraction at the surface was obtained from the vapor pressure curve for a given total pressure. A second relation was obtained from the gas phase model (either infinite activation energy or unity Lewis number). The point where the two relations were simultaneously satisfied gave the unique solution for the liquid surface temperature and surface fuel mole fraction for a given total pressure.

Results:

The burning rate results for hydrazine are summarized in Figure 9. For the highest purity hydrazine tested, the burning rate varied linearly with pressure for all tube sizes except for the lowest pressures tested where a slight fall off from the linear relation occurred. As pressure increased the tube size had less effect on the burning rate but the liquid concentration had a significant effect.

The purity of the hydrazine sample was obtained by commercial gas chromatographic analysis. This analysis indicated that the sample was made up of 98.6% hydrazine, 1.3% water and 0.1% trace impurities, by volume. The purity of the other samples of hydrazine shown on Figure 9 was obtained by water dilution of the 98.6% sample.

The upper limit in pressure shown on Figure 9 was the highest pressure for which hydrazine would steadily propagate. Upper extinction pressures for the stand burning of hydrazine have previously been noted by other investigators (18, 19, 20). As indicated on Figure 9, the upper extinction pressure varied with tube size and also liquid concentration.

The liquid surface temperature results are shown on Figure 10. As expected, the low pressure phase equilibrium model was quite adequate for hydrazine since the pressure levels tested were well below the critical pressure. Also evident from Figure 10 is that the two different gas phase models predict nearly identical results and both predictions agree quite well with the experimental values.

Summary and Conclusions:

The burning rates and surface temperatures of liquid strands of hydrazine have been measured for various pressures. Burning rates were obtained over the pressure range of 7 to 600 psia and were found to increase linearly with pressure except for subatmospheric pressures. The

concentration water in liquid hydrazine has a significant effect on the burning rate particularly at high pressures. Smaller tube diameters were found to cause an increase in the apparent burning rate, particularly at low pressures.

Surface temperatures of burning liquid strands of hydrazine were measured in the pressure range of 7 to 300 psia. The low pressure phase equilibrium model with and without using the unity Lewis number assumption predicts the experimental data quite well over the entire pressure range.

V. Oscillatory Combustion

Introduction:

This portion of the investigation concerns the influence of pressure transients on the combustion of a liquid monopropellant fuel. The combustion system consists of a liquid surface from which fuel evaporates; as the gaseous fuel flows away from the liquid surface, it undergoes exothermic chemical decomposition. A portion of the heat evolved in the decomposition process flows back to the liquid surface providing the energy for further evaporation of the liquid. The remainder of the energy released is convected downstream by the gas flow. The main thrust of the present work is to gain an understanding of the coupling between an oscillatory pressure wave and the fuel burning rate.

Numerous theories have been developed to predict the response of a burning liquid to pressure oscillations. However, direct experimental measurements of this phenomenon are lacking. The purpose of this study is to obtain experimental data on the response of a burning monopropellant to an oscillating pressure environment and to compare these results with a theoretical model of the system.

An important criterion must be met if an adequate test of any theoretical response model is to be made. For a burning liquid, the characteristic frequency of thermal wave propagation in the liquid phase can be defined as m^2/α where m is the mean burning rate of the fuel and α is the liquid phase thermal diffusivity. For pressure oscillation frequencies much less than this characteristic frequency, the system behaves quasi-steadily. This frequency regime provides a relatively weak test of theoretical response models. Therefore, pressure oscillation frequencies should be at least the same order of magnitude as the liquid phase critical frequency for at least a portion of the experimental data.

The steady strand study indicated that the burning rate, m, of hydrazine is roughly proportional to pressure. Since α for hydrazine is nearly independent of pressure, the characteristic frequency decreases with decreasing pressure. Quasi-steady analysis indicated that low mean pressures produce larger surface oscillations for a given pressure amplitude (16). Thus low pressures are favored as the condition where the response of the liquid can be observed throughout the entire frequency range of interest. Since hydrazine will burn as a liquid strand at low pressures, this fuel is particularly suited for measurements of burning rate response and it was chosen as the fuel to be studied.

During this report period an oscillatory pressure version of the steady strand apparatus was assembled and preliminary testing was begun. Also, the theoretical model was formulated and the resulting equations derived. These equations are now being coded for computer solution.

Experimental Apparatus:

The oscillatory combustion apparatus is shown in Figure 11. The major components are the glass tube filled with liquid monopropellant fuel, the camera-lens system used to measure the fluctuations of the burning liquid surface to the imposed pressure oscillations and the rotary valve arrangement used to provide the oscillatory pressure variations. The fuel ignition system is similar to the one used in the steady strand study.

The rotary valve arrangement is similar to the system described in Reference 21 for establishing an oscillating propane gas flame. With this technique an oscillating pressure is set up in the test chamber by an oscillating air stream.

The oscillating air stream is produced through the use of a ball valve and needle valve mounted in parallel. The amplitude of the oscillating pressure can be varied independently of the frequency by varying the relative amounts of air passing through the two valves. The frequency is varied by varying the speed of the DC motor used to rotate the ball valve. The mean pressure in the chamber can be varied by the setting of the needle valve in the exhaust line. For testing at subatmospheric pressures, the exhaust line is connected to a large chamber which is in turn connected to a vacuum pump.

Quasi-steady analysis indicates that typical liquid surface oscillation amplitudes are on the order of 0.01 mm (16). In order to resolve such small distances, the camera-lens system shown on Figure 11 is used in conjunction with a Vanguard motion analyzer. The camera is a 35 mm strip camera and the lens has a focal length of 150 mm. Primary gains as high as 5:1 have been obtained with this system. This gain coupled with the gain of about 20:1 of the Vanguard provides an overall gain of 100:1 which is adequate for accurate resolution of the film records.

Any phase shift between the imposed pressure oscillations and the resulting burning rate oscillations are determined from the films and the pressure trace registered on an oscillograph. The film and pressure records are synchronized by a switch closure which deflects a galvanometer on the pressure record and starts a light streak on the film. Timing marks are placed on both the film and pressure record.

Theoretical Analysis:

Existing Theories

A number of theories have been developed to determine the response of burning liquids to imposed pressure and velocity fluctuations (22-24, to name only a few). However, none of the current liquid surface response models provide for a monopropellant gas phase combustion process. Earlier work on the combustion of hydrazine indicates that a monopropellant gas phase model is more realistic for the hydrazine fuels under rocket engine conditions (25).

Since the process is one dimensional, some insight into the modeling of the experiment can be gained by studing solid propellant combustion instability theories (26-31 are representative). In particular, neglecting condensed phase reactions, solid propellant models are applicable to the present problem with modified boundary conditions at the two phase interface and slight modifications of the gas phase analysis. Although the present theoretical model is of the one-dimensional experiment, the results should lead to a better understanding of liquid response and thus to improved droplet response models.

General Model

A sketch of the theoretical model is shown on Figure 12. The coordinate system chosen is inertial with the origin at the mean position of the burning surface (28-29). With the imposed sinusoidal pressure oscillations, x_s, the instantaneous position of the liquid surface, varies as shown in Figure 12 to first order in pressure amplitude. The steady state temperature, fuel mass fraction and gas phase reaction rate profiles are also shown on Figure 12.

For generality, the gas phase transient effects have been included in the analysis similar to the approach used by T'ien for solid propellants (31). Also included are the effects of variable properties through the introduction of a modified Howarth transformation.

The major assumptions used in the analysis are as follows:

1. The flow is one-dimensional with a Mach number much less than unity and all body forces are negligible.

2. The flame is premixed and laminar. A one-step, irreversible chemical reaction takes place in the reaction zone and any time lags associated with the chemical reaction itself are negligible.

3. Radiation heat transfer is negligible. An estimation of the radiation contribution indicates that it accounts for less than 1% of the total energy required for the vaporization of hydrazine under steady state conditions. This is not surprising since hydrazine has a low adiabatic flame temperature.

4. With regard to thermodynamic properties, it is assumed that all gas phase diffusion coefficients are equal, all molecular weights are equal and constant, all gas phase specific heats are equal and constant, the gas phase mixture thermal conductivity varies linearly with temperature but is independent of composition, and the liquid is composed of a single chemical species with constant properties.

5. Since the pressure levels are low, the combustion products are taken to be insoluble in the liquid phase. Chemical reaction is also neglected in the liquid phase.

6. Based on the steady strand study, the Lewis number is assumed to be unity.

7. The gas phase is taken to be an ideal gas and at the liquid surface the surface fuel mass fraction is related to the surface temperature through the Clausius-Clapeyron equation.

8. Since the Mach number is much less than unity, the inertial and viscous terms in the momentum equation are neglected.

9. The complete unsteady gas phase equations are used but the wavelength of any periodic pressure disturbance is assumed to be long compared to the distance from the outer edge of the reaction zone to the liquid surface. Estimation indicates that this assumption is valid for frequencies up to about 50,000 Hz. Assumptions 8 and 9 indicate that pressure is only a function of time.

Thus, the theoretical model includes the effects of time dependent heat and mass transfer in both the liquid and gas phases. Variable property effects are also included in the gas phase. Global kinetic parameters are used to characterize the hydrazine decomposition flame.

Governing Equations

With the above assumptions, the equations of overall continuity, species conservation and energy in the gas phase and overall continuity and energy in the liquid phase were obtained from the general equations given by Williams (32).

For the gas phase the equations are*:

Gas Phase, $x_s^*(t^*) < x^* < \infty$

Conservation of Mass

$$\frac{\partial \rho^*}{\partial t^*} + \frac{\partial \rho^* v^*}{\partial x^*} = 0 \tag{1}$$

Conservation of Species

$$\rho^* \frac{\partial Y_i}{\partial t^*} + \rho^* v^* \frac{\partial Y_i}{\partial x^*} - \frac{\partial}{\partial x^*}\left(\rho^* D \frac{\partial Y_i}{\partial x^*}\right) = \sqrt{_i} w^*_F \tag{2}$$

Conservation of Energy

$$\rho^* C_p \frac{\partial T^*}{\partial t^*} + \rho^* v^* C_p \frac{\partial T^*}{\partial x^*} - \frac{\partial}{\partial x^*}\left(\lambda^* \frac{\partial T^*}{\partial x^*}\right) - \frac{\partial p^*}{\partial t^*} = q^* w^*_F \tag{3}$$

Since the gas is ideal

$$p^* = \rho^* R T^* \tag{4}$$

*See the nomenclature at the end of this section for the meaning of symbols.

In Equations (2) and (3) the following definitions have been used:

$$w_F^* = B^* T^{*\delta} \left(\frac{P^*}{RT^*}\right)^n \left(\frac{Y_F}{M_F}\right)^n \exp \left(\frac{-E^*}{RT^*}\right) \tag{5}$$

$$q^* = -\sum_{i-1}^{n} h_i^o \frac{\nu_i'' M_i}{\nu_i' M_F} \tag{6}$$

$$\nu_i = \frac{(\nu_i'' - \nu_i') M_i}{\nu_F' M_F} \tag{7}$$

Here w_F^* is the rate of reaction of the fuel with a pre-exponential factor of $B^* T^{*\delta}$ and an activation energy of E^*, q^* is the heat of combustion and ν_i is related to the stoichiometric coefficients.

The equations of conservation of mass and energy in the liquid phase are:

Liquid Phase, $-\infty < x^* < x_s^* (t^*)$

Conservation of Mass

$$v_\ell^* = \text{constant} \tag{8}$$

Conservation of Energy

$$\rho^* C_\ell \frac{\partial T^*}{\partial t^*} + \rho_\ell^* v_\ell^* C_\ell \frac{\partial T^*}{\partial x^*} - \lambda_\ell^* \frac{\partial^2 T^*}{\partial x^{*2}} = 0 \tag{9}$$

Since only oscillatory solutions are required, the initial conditions are irrelevant. The boundary conditions applicable to the present problem can be summarized as follows. At the cold end of the liquid propellant, the temperature must be constant with respect to both x^* and t^*.

$$x^* \to -\infty$$
$$T^* \to T^*_{-\infty} \quad \text{(a constant)} \tag{10}$$

At the liquid surface $x_s^*(t^*)$ six conditions must be satisfied. The first two are obvious and are mentioned only for completeness. That is, the temperature and pressure must be continuous across the surface.

$$T^*_{s^-} = T^*_{s^+} \tag{11}$$

$$p^*_{s^-} = p^*_{s^+} \tag{12}$$

Conservation of mass applied across the moving surface reduces to:

$$\rho_\ell^* (v_\ell^* - \dot{x}_s^*) = \rho^*(v^* - \dot{x}_s^*) \tag{13}$$

and conservation of energy at the surface yields:

$$\lambda_\ell^* \left(\frac{\partial T^*}{\partial x^*}\right)_{s^-} = \left[\lambda^* \frac{\partial T^*}{\partial x^*}\right]_{s^+} - \rho_\ell^*(v_\ell^* - \dot{x}_s^*) [(C_p - C_\ell)T_s^* + L^*] \tag{14}$$

Since the products of combustion are assumed to be insoluble in the liquid phase, the gradient of the fuel mass fraction is related to the fuel mass fraction at the liquid surface as follows:

$$\left(\rho^*D \frac{\partial Y_F}{\partial x^*}\right)_{s^+} = \rho_\ell^*(v_\ell^* - \dot{x}_s^*) (Y_{F,s} - 1) \tag{15}$$

The Clausius-Clapeyron equation relates the fuel mass fraction at the surface to the surface temperature.

$$Y_{F,s} = \frac{a^*}{p^*} \exp \left(\frac{-L^*}{RT_s^*}\right) \tag{16}$$

where L* is the heat of vaporization of the fuel and a* is a constant with the dimensions of pressure. The remaining boundary conditions relate the variation of fuel mass fraction and temperature far from the liquid surface. Far from the surface, the gas phase chemical reaction must go to completion since eventually all the fuel will react. Thus,

$$x^* \to \infty$$
$$Y_F \to 0 \tag{17}$$

for all time. In addition, the temperature must become independent of x* since the only energy source, the chemical reaction, has gone to completion and heat conduction will smooth out any temperature variations with respect to distance. However, the temperature will still vary with time since the pressure is a function of time. Therefore:

$$x^* \to \infty$$
$$T^*(x^*, t^*) \to T_\infty^*(t^*) \tag{18}$$

where $T_\infty^*(t^*)$ is a known function.

Equations 1-18 are placed in dimensionless form by introducing the following variables.

$$\rho = \frac{\rho^*}{\rho^*_{\infty 0}} \qquad\qquad T = \frac{T^*}{T^*_{\infty 0}} \qquad\qquad v = \frac{v^*}{v^*_{\infty 0}}$$

$$P = \frac{P^*}{P^*_0} \qquad\qquad \lambda = \frac{\lambda^*}{\lambda^*_{\infty 0}} \qquad\qquad t = \frac{t^* \rho^*_{\infty 0} C_p v^{*2}_{\infty 0}}{\lambda^*_{\infty 0}} \qquad (19)$$

$$x = \frac{x^* \rho^*_{\infty 0} C_p v^*_{\infty 0}}{\lambda^*_{\infty 0}}$$

The subscript ∞o signifies a zero order (steady state) quantity evaluated at infinity.

Treatment of variable gas phase properties is accomplished by the Howarth Transformation appropriate to the present coordinate system by defining

$$\eta = \frac{C_p v^*_{\infty 0}}{\lambda^*_{\infty 0}} \int_{x^*_s(t^*)}^{x^*} \rho^* dx^* \qquad (20)$$

and by defining a modified mass flux as

$$r = \rho v + \frac{\partial}{\partial t} \int_{x_s(t)}^{x} \rho\, dx \qquad (21)$$

The Shvab-Zeldovich variable θ, is also introduced as a dependent variable.

$$\theta = qY_F + T \qquad (22)$$

Substituting equations 19-22 into equations 1-4 then yields:

Gas Phase, $0 < \eta < \infty$

$$\frac{\partial r}{\partial \eta} = 0 \qquad (23)$$

$$\frac{\partial \theta}{\partial t} + r \frac{\partial \theta}{\partial \eta} - P \frac{\partial^2 \theta}{\partial \eta^2} - \left(\frac{\gamma-1}{\gamma}\right) \frac{1}{\rho} \frac{\partial P}{\partial t} = 0 \qquad (24)$$

$$\frac{\partial T}{\partial t} + r \frac{\partial T}{\partial \eta} - P \frac{\partial^2 T}{\partial \eta^2} - \left(\frac{\gamma-1}{\gamma}\right) \frac{1}{\rho} \frac{\partial P}{\partial t} = qw \qquad (25)$$

$$P = \rho T \qquad (26)$$

In deriving Equations (24) and (25) use has been made of the fact that $\nu_F = -1$ for the present case. The dimensionless reaction rate is

defined as

$$w = \frac{A}{q^n} T^{1 + \delta - n} p^{n - 1} (\theta - T)^n \exp\left(\frac{-E}{T}\right) \tag{27}$$

where E is the dimensionless activation energy,

$$E = \frac{E^*}{RT^*_{\infty O}} \tag{28}$$

q is the dimensionless heat of combustion

$$q = \frac{q^*}{C_p T^*_{\infty O}} \tag{29}$$

and A is related to the pre-exponential factor and zero order mass flux

$$A = \frac{B^* T^{*\delta}_{\infty O} \lambda^*_{\infty O}}{\rho^2_{\infty O} v^2_{\infty O} C_p} \left(\frac{p^*_O}{M_F RT^*_{\infty O}}\right)^n \tag{30}$$

Also, noting that

$$\frac{\lambda^*}{\lambda^*_{\infty O}} = \frac{T^*}{T^*_{\infty O}} \tag{31}$$

and through the use of the ideal gas equation of state, it follows that

$$\rho \lambda = P \tag{32}$$

The dimensionless liquid phase continuity and energy equations are
Liquid Phase, $-\infty < \eta < 0$

$$r = r(t) \tag{33}$$

$$\frac{\partial T}{\partial t} + r \frac{\partial T}{\partial \eta} - \delta_1 \frac{\partial^2 T}{\partial \eta^2} = 0 \tag{34}$$

The dimensionless parameter δ_1 is a constant defined as

$$\delta_1 = \frac{\rho_\ell \lambda_\ell C_p}{C_\ell} \tag{35}$$

The nondimensional boundary conditions are as follows. At the cold end of the fuel,

$$\eta \rightarrow -\infty$$
$$T(\eta, t) \rightarrow T_{-\infty} \tag{36}$$

At the liquid surface, the conservation of mass yields

$\eta = 0$

$$r(t) = \rho(o) [v(o) - \dot{x}_s] = \rho_\ell (v_\ell - \dot{x}_s) \qquad (37)$$

The conservation of energy across the surface becomes

$$\rho_\ell \lambda_\ell \left(\frac{\partial T}{\partial \eta}\right)_{\eta = o^-} = P\left(\frac{\partial T}{\partial \eta}\right)_{\eta = o^+} - r[T(o) (1-\beta) + L] \qquad (38)$$

where β is the ratio of liquid to gas specific heats

$$\beta = \frac{C_\ell}{C_p} \qquad (39)$$

and L is the nondimensional heat of vaporization

$$L = \frac{L^*}{C_p T^*_{\infty o}} \qquad (40)$$

The insolubility condition requires that

$$P\left(\frac{\partial \theta}{\partial \eta}\right)_{\eta = o^+} = r[\theta(o) - T(o) - q] + P\left(\frac{\partial T}{\partial \eta}\right)_{\eta = o^+} \qquad (41)$$

The Clausius-Clapeyron equation after nondimensionalization is

$$\theta(0) = \frac{aq}{P} \exp\left[\frac{-L}{T(0)}\right] + T(0) \qquad (42)$$

where

$$a = \frac{a^*}{P^*_o} \qquad (43)$$

The dimensionless conditions far from the surface reduce to

$\eta \to \infty$

$$\theta(\eta, t) \to T(\eta, t) \to T(t) \qquad (44)$$

where T(t) is a specified function.

To solve the system of partial differential equations, Equations (23-25) and (34), with the given boundary conditions, it is assumed that all amplitudes of oscillation are small, allowing the use of a perturbation analysis. For oscillatory solutions, the dependent variables can be expressed as

$$P(t) = 1 + \epsilon e^{i\omega t}$$

$$T(\eta, t) = T_o(\eta) + \epsilon T_1(\eta) e^{i\omega t}$$

$$\theta(\eta, t) = \theta_o(\eta) + \epsilon \theta_1(\eta) e^{i\omega t} \qquad (45)$$

$$r(t) = r_o + \epsilon r_1 e^{i\omega t}$$

$$x_s(t) = 0 + \epsilon x_{s1} e^{i\omega t}$$

where ϵ represents the normalized amplitude of the imposed pressure oscillations. Substituting Equation (45) into Equations (23-25) and (34) and the boundary conditions, the resulting equations are separated in terms of powers of $\epsilon e^{i\omega t}$.

Zero Order (Steady State) Problem

For the zero order problem, the gas phase can be solved independently of the liquid phase. The problem reduces to the following:

Gas Phase, $0 < \eta < \infty$

$$\frac{d^2 T_o}{d\eta^2} - \frac{dT_o}{d\eta} + q^{1-n} A T_o^{1+\delta-n} (1-T_o)^n \exp\left(\frac{-E}{T_o}\right) = 0 \qquad (46)$$

with the boundary conditions

$\eta \to \infty$

$$T_o \to 1 \qquad (47)$$

and at $\eta = 0$

$$\left(\frac{dT_o}{d\eta}\right)_{\eta = 0^+} = q + T_o(0) - 1 \qquad (48)$$

$$T_o(0) = 1 - aq \exp\left[\frac{-L}{T_o(0)}\right] \qquad (49)$$

In Equations (46-49) use has been made of the conservation of mass requirement that

$$r_o = constant = \rho_{\infty o} v_{\infty o} = 1 \qquad (50)$$

and also that

$$\theta_o(\eta) = 1 \qquad (51)$$

from Equations (24) and (45).

In Equation (46), A is unknown since it is related to the burning rate $\rho_{\infty 0}^{*} \, v_{\infty 0}^{*}$ which is unknown. The three boundary conditions permit a unique value of A to be determined.

First Order Problem

The liquid phase solution is required for the complete specification of the first order problem. To zero order in ε, the equation and boundary conditions are:

Liquid Phase, $-\infty < \eta < 0$

$$\delta_1 \frac{d^2 T_0}{d\eta^2} - \frac{dT_0}{d\eta} = 0 \tag{52}$$

$$\eta \to -\infty \qquad T_0 \to T_{-\infty}$$

$$\eta = 0 \qquad T_0 = T_0(0) \tag{53}$$

The solution of Equation (52) subject to the boundary conditions of Equation (53) is

$$T_0 = T_{-\infty} + [T_0(0) - T_{-\infty}] \exp(\eta/\delta_1) \tag{54}$$

To first order in ε the equation and boundary conditions for the liquid phase are:

$$\delta_1 \frac{d^2 T_1}{d\eta^2} - \frac{dT_1}{d\eta} - i\omega T_1 = r_1 \frac{dT_0}{d\eta} \tag{55}$$

$$\eta \to -\infty \qquad T_1 \to 0$$

$$\eta = 0 \qquad T_1 = T_1(0) \tag{56}$$

The solution of the first order system is

$$T_1 = \left\{ T_1(0) + \frac{r_1}{\delta_1 i\omega} [T_0(0) - T_{-\infty}] \right\} \exp \left(\frac{1 + \sqrt{1 + 4 i\omega \delta_1}}{2\delta_1} \eta \right)$$

$$\frac{-r_1}{\delta_1 i\omega} [T_0(0) - T_{-\infty}] \exp(\eta/\delta_1) \tag{57}$$

The first order gas phase equations reduce to the following.

Gas Phase, $0 < \eta < \infty$

$$r_1 = \text{constant} \tag{58}$$

$$\frac{d^2\theta_1}{d\eta^2} - \frac{d\theta_1}{d\eta} - i\omega\theta_1 = - \left[\frac{\gamma - 1}{\gamma}\right] i\omega \tag{59}$$

$$\frac{d^2T_1}{d\eta^2} - \frac{dT_1}{d\eta} + T_1\{qw_o \left| \left(\frac{1 + \delta - n}{T_o}\right) - \frac{n}{1 - T_o} + \frac{E}{T_o^2} \right| - i\omega\}$$

$$+ \frac{nqw_o}{1 - T_o} \theta_1 = (r_1 + 1) \frac{dT_o}{d\eta} - 2 \frac{d^2T_o}{d\eta^2} - \left[\frac{\gamma-1}{\gamma}\right] i\omega T_o - nqw_o \tag{60}$$

In Equation (60) w_o is defined by the following expression:

$$w_o = \frac{A}{q^n} T_o^{1 + \delta - n} (1 - T_o)^n \exp\left[\frac{-E}{T_o}\right] \tag{61}$$

Using Equation (57) the conservation of energy boundary condition to first order in ϵ becomes

$\eta = 0$

$$\left(\frac{dT_1}{d\eta}\right)_{\eta = 0^+} = r_1\{\frac{\rho_\ell \lambda_\ell}{2\delta_1^2} i\omega[T_o(0) - T_{-\infty}] [\sqrt{1+4i\omega\delta_1} - 1] + T_o(0) (1-\beta) + L\}$$

$$+ T_1(0) [1-\beta + \frac{\rho_\ell \lambda_\ell}{2\delta_1} (1 + \sqrt{1+4i\omega\delta_1})] - \left(\frac{dT_o}{d\eta}\right)_{\eta = 0^+} \tag{62}$$

The Clausius - Clapeyron equation reduces to

$$\theta_1(0) = aq \frac{T_1(0)}{T_o^2(0)} \exp\left|\frac{-L}{T_o(0)}\right| + T_o(0) + T_1(0) - 1 \tag{63}$$

and the insolubility condition requires that

$$\left(\frac{d\theta}{d\eta}\right)_{\eta = 0^+} = r_1[1-T_o(0)-q] + \theta_1(0) - T_1(0) + \left(\frac{dT_1}{d\eta}\right)_{\eta=0^+} + \left(\frac{dT_o}{d\eta}\right)_{\eta=0^+} \tag{64}$$

The outer boundary conditions from Equation (47) are

$\eta \to \infty$

$$\theta_1(\eta) \to T_1(\eta) \to \text{a constant} \qquad (65)$$

The constant in Equation (65) can be determined by solving Equation (59). It is easily verified that as $\eta \to \infty$,

$$\theta_1(\eta) \to T_1(\eta) \to \frac{\gamma - 1}{\gamma} \qquad (66)$$

which is the form for isentropic flow.

Now consider how the theoretical results can be compared to the experiment results. For the zero order (steady state) problem, the steady strand measurements provide steady state burning rates and liquid surface temperatures. By matching theory with experiment, realistic global kinetic parameters (activation energy and pre-exponential factor) can be determined for given thermodynamic properties.

For the unsteady case, ϵ, the expansion parameter, is related to the amplitude of the imposed pressure oscillations. Since r_1 is related to the unsteady burning rate in response to these imposed pressure oscillations, it remains to be shown how r_1 is related to the unsteady burning rate measured in the experiment.

From the conservation of mass at the liqud surface, Equation (37), and Equation (45) it follows that

$$r_1 = -\rho_\ell \, i\omega x_{s1} \qquad (67)$$

Rearranging Equation (67)

$$x_{s1} = \frac{-r_1}{\rho_\ell i\omega} \qquad (68)$$

Since ρ_ℓ is a given thermodynamic property, x_{s1} is directly related to r_1. Moreover, x_{s1} is a complex number with both amplitude and phase parameters. Both of these parameters can be directly compared with the measured amplitude of the liquid surface oscillations and the phase lag of these oscillation with respect to the pressure oscillations.

At the present time the equations are being coded for computer solution. The zero order theoretical solution will be matched to the steady strand work to determine realistic global kinetic parameters. Using these same parameters, the first order equations will be solved to determine the predicted burning rate fluxuations. These predicted values will then be directly compared to the unsteady experimental burning rate results.

Summary and Conclusions:

The experimental apparatus has been assembled and preliminary testing has begun. During the coming report period, the burning rate response of hydrazine will be measured for various imposed pressure wave amplitudes and frequencies of oscillation. The frequency range tested will include, at least, frequencies of the same order of magnitude as the liquid phase critical frequency. In nondimensional form this corresponds to ω on the order of 10^{-3} to 10^{-2}.

The oscillatory theory has been developed through first order in amplitude of the pressure oscillations. The resulting equations are being coded for computer solution. The theoretical predictions will be compared to the experimental results to provide a direct test of the model.

Nomenclature, Section V

Symbol	Description
A	Defined in Equation (30)
a	Constant in Clausius-Clapeyron Equation, see Equation (16)
B*	Pre-exponential factor
C_ℓ	Specific heat of liquid
C_p	Specific heat of gas
D	Diffusion coefficient
E	Activation energy
h_i^o	Standard heat of formation of species i
i	$\sqrt{-1}$
L	Heat of vaporization
M	Molecular weight
m	Mean burning rate
N	Total number of species
n	Reaction order

Symbol	Description
p	Pressure
q	Heat of combustion
R	Gas constnat
r	Defined in Eq. (21)
T	Temperature
$T_{-\infty}$	Temperature of cold end of liquid fuel
t	Time
v	Velocity
w	Reaction rate
x	Distance
x_s	Instantaneous position of liquid surface
Y	Mass fraction
α	Liquid diffusivity
β	Ratio of specific heats, see Eq. (39)
γ	Specific heat ratio
δ	Temperature dependence of pre-exponential factor
δ_1	Defined by Eq. (35)
ϵ	Amplitude of oscillatory pressure
η	Dimensionless distance, see Eq. (20)
θ	Defined by Eq. (22)
λ	Thermal conductivity
ν_i	Defined by Eq. (7)
ν_i'	Stoichiometric coefficient of species i as reactant
ν_i''	Stoichiometric coefficient of species i as product
ρ	Density
ω	Nondimensional frequency

Subscripts	Description
F	Fuel
i	Species i
ℓ	Liquid
s	Liquid surface
s^-	Inner side of liquid surface
s^+	Outer side of liquid surface
o	Steady State quantities
1	First order quantities
∞	Far from liquid surface

Supercripts	
*	Dimensional quantities

REFERENCES

1. Canada, G. S. and G. M. Faeth, "Fuel Droplet Burning Rates at High Pressures," Fourteenth Symposium (International) on Combustion, The Pennsylvania State University, University Park, Pennsylvania, August 1972, to be published.

2. Anderson, J. W. and R. Friedman, "An Accurate Metering System for Laminar Flow Studies," The Review of Scientific Instruments, Vol. 20, No. 1, January 1950, p. 66.

3. Lazar, R. S. and G. M. Faeth, "Bipropellant Droplet Combustion in the Vicinity of the Critical Point," Thirteenth Symposium (International) on Combustion, The Combustion Institute, Pittsburgh, Pennsylvania, 1971, pp. 743-753.

4. Lazar, R. S., "Bipropellant Droplet Combustion in the Vicinity of the Critical Point," Ph.D. Thesis, The Pennsylvania State University, 1970.

5. Faeth, G. M. and R. S. Lazar, "Fuel Droplet Burning Rates in a Combustion Gas Environment," AIAA J., Vol. 9, No. 11, 1971, pp. 2165-2171.

6. Williams, F. A., Combustion Theory, p. 56, Addison-Wesley, 1965.

7. Yuge, T., "Experiments on Heat Transfer from Spheres including Combined Natural and Forced Convection," ASME Transactions, Vol. 82, Series C, 1960, pp. 214-220.

8. Spalding, D. B., "The Combustion of Liquid Fuels," Fourth Symposium (International) on Combustion, Williams and Wilkins, Baltimore, 1953, pp. 847-864.

9. Reid, R. C. and T. K. Sherwood, The Properties of Gases and Liquids, 2nd Edition, p. 596, McGraw-Hill, 1966.

10. Prausnitz, J. M. and Chueh, P. L., Computer Calculations for High Pressure Vapor-Liquid Equilibria, p. 18, Prentice-Hall, 1968.

11. Fristrom, R. and A. Westenberg, Flame Structure, pp. 170-174, McGraw-Hill, 1965.

12. Fendell, F. E., et.al., "Thin-Flame Theory for a Fuel Droplet in Slow Viscous Flow," Journal of Fluid Mechanics, Vol. 126, Part 2, 1966, pp. 267-280.

13. Frossling, N., "Uber die Verdunstung Fallender Tropfen," Bertrag. Geophysics, Vol. 52, 1938, pp. 170-216.

14. Allender, C., Transactions Royal Institute of Technology, No. 70, Stockholm, Sweden, 1953.

15. Faeth, G. M., "High-Pressure Liquid-Monopropellant Strand Combustion," Combustion and Flame, Vol. 18, 1972, pp. 103-113.

16. Allison, C. B., Canada, G. S. and Faeth, G. M., "1971 Annual Report on the Investigation of Critical Burning of Fuel Droplets," NASA CR-120879, January 1972.

17. Jones, W. H. (Chairman), JANNAF Thermochemical Tables, Dow Chemical Company, Midland, Michigan.

18. Antoine, A. C., "The Mechanism of Burning of Liquid Hydrazine," Eighth Symposium (International) on Combustion, Williams and Wilkins, Baltimore, 1962, pp. 1057-1059.

19. Adams, G. and Stocks, G. W., "The Combustion of Hydrazine," Fourth Symposium (International) on Combustion, Williams and Wilkins, Baltimore, 1953, pp. 239-248.

20. Gray, P. and Kay, J. C., "Stability of the Decomposition Flame of Liquid Hydrazine," Research, London, Vol. 8, 1955, pp. 53-55.

21. Chervinsky, A. P. Sirignano, W. A., Harrje, D. T. and Varma, A. K., "Axisymmetric Jet Diffusion Flame in an External Oscillating Stream," Sixth ICRPG Combustion Conference, CPIA Publication No. 192, December 1969.

22. Heidmann, M. F. and Wieber, P. R., "Analysis of Frequency Response Characteristics of Propellant Vaporization," AIAA Paper No. 66-604, 1966.

23. Strahle, W. C., "A Transient Problem on the Evaporation of a Reactive Fuel," Combustion Science and Technology, Vol. 1, 1969, pp. 25-33.

24. T'ien, J. S. and Sirignano, W. A., "Unsteady Thermal Response of the Condensed Phase Fuel Adjacent to a Reacting Gaseous Boundary Layer," Thirteenth Symposium (International) on Combustion, The Combustion Institute, Pittsburgh, Pa., 1971, pp. 529-539.

25. Allison, C. B. and Faeth, G. M. "Decomposition and Hybrid Combustion of Hydrazine, MMH and UDMH as Droplets in a Combustion Gas Environment," Combustion and Flame, Vol. 19, October 1972, pp. 213-226.

26. Hart, W. R. and McClure, F. T., "Combustion Instability: Acoustic Interaction with a Burning Propellant Surface," Journal of Chemical Physics, Vol. 30, September 1959, pp. 1501-1514.

27. Denison, M. R. and Baum, E., "A Simplified Model of Unstable Burning in Solid Propellants," ARS Journal, Vol. 31, No. 18, August 1961, pp. 1112-1122.

28. Williams, F. A., "Response of a Burning Solid to Small Amplitude Pressure Oscillations," Journal of Applied Physics, Vol. 33, November 1962, pp. 3153-3166.

29. Culick, F. E. C., "Calucation of the Admittance Function for a Burning Surface," Astronautics Acta, Vol. 13, 1967, pp. 221-237.

30. Krier, H., et.al., "Nonsteady Burning Phenomena of Solid Propellants: Theory and Experiment," AIAA Journal, Vol. 6, No. 2, February 1968, pp. 278-285.

31. T'ien, J. S., "Oscillatory Burning of Solid Propellants including Gas Phase Time Lag," Combustion Science and Technology, Vol. 5, 1972, pp. 47-54.

32. Williams, F. A., Combustion Theory, Addison-Wesley, Reading, Massachusetts, 1965, Chapter 1.

Table I

Predicted Critical Burning Conditions for Porous Sphere Combustion in Air*

Substance	CH_3OH	C_2H_5OH	C_3H_7OH	C_5H_{12}	C_7H_{16}	$C_{10}H_{22}$
Critical Properties						
Pressure	78.5	63.0	51.0	33.3	27.0	20.8
Temperature	513.2	516.0	540.7	469.5	540.2	619.0
Low Pressure Theory						
Total Pressure	109	88	78	48	52	51
Surface Temperature	513.2	516.0	540.7	469.5	540.2	619.0
Binary High Pressure Theory						
Total Pressure	168	125	125	82	108	125
Surface Temperature	489	496	516	450	512	590
Quaternary High Pressure Theory						
Total Pressure	114	100	102	65	80	108
Surface Temperature	486	494	514	449	510	583

*Fuel inlet and ambient air temperature of 300°K, pressure in atm, temperatures in K.

FIG. 1 HIGH PRESSURE COMBUSTION APPARATUS.

TO EXHAUST

WATER TRAP

BLOWOFF VALVE

PRESSURE CONTROL VALVE

FUEL SUPPLY

HEAT EXCHANGER

INSULATION

MEASURING BURETTE

WINDOW

PROBE

DRIP PAN

FUEL PUMP

RELIEF VALVE

REACTOR PRESSURE

IGNITER

AIR

FLOW ORIFICE

GAS PRESSURE

TO COMPRESSOR

31
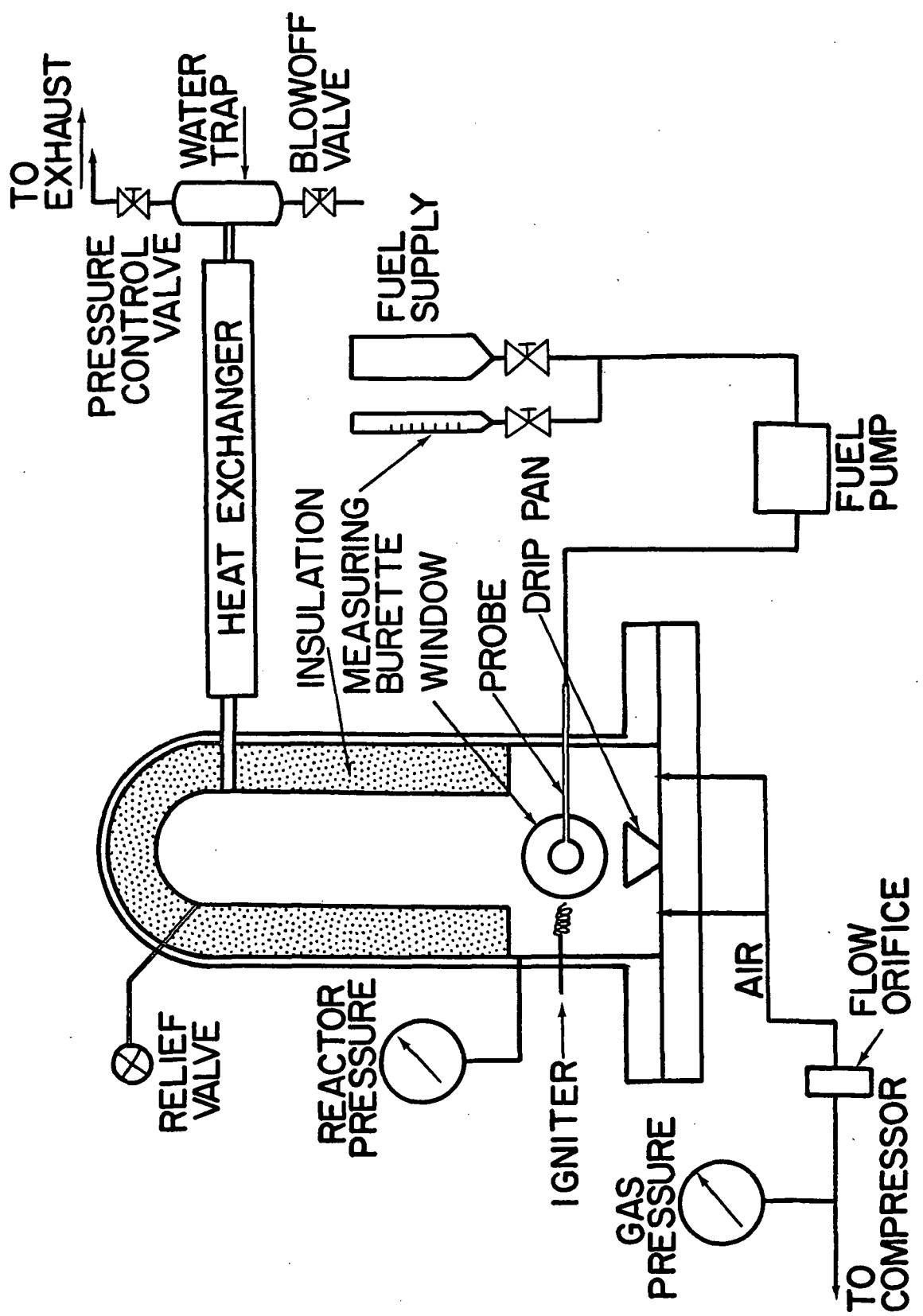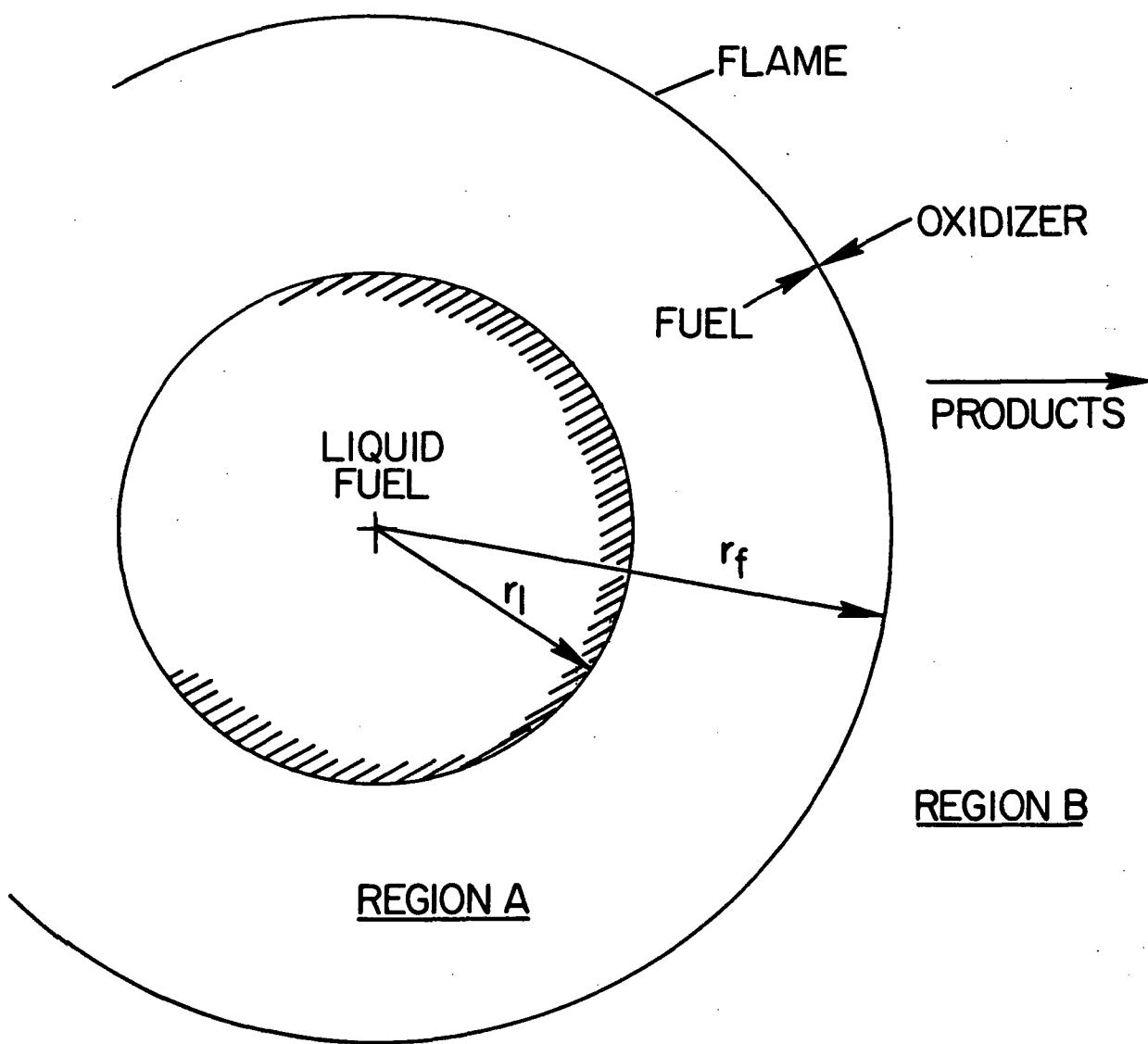
FIG. 2   MODEL OF THE BURNING OF A FUEL DROPLET IN AN OXIDIZING
ATMOSPHERE.

3γ

FIG. 3 EXPERIMENTAL BURNING RATES FOR ALCOHOLS.

34
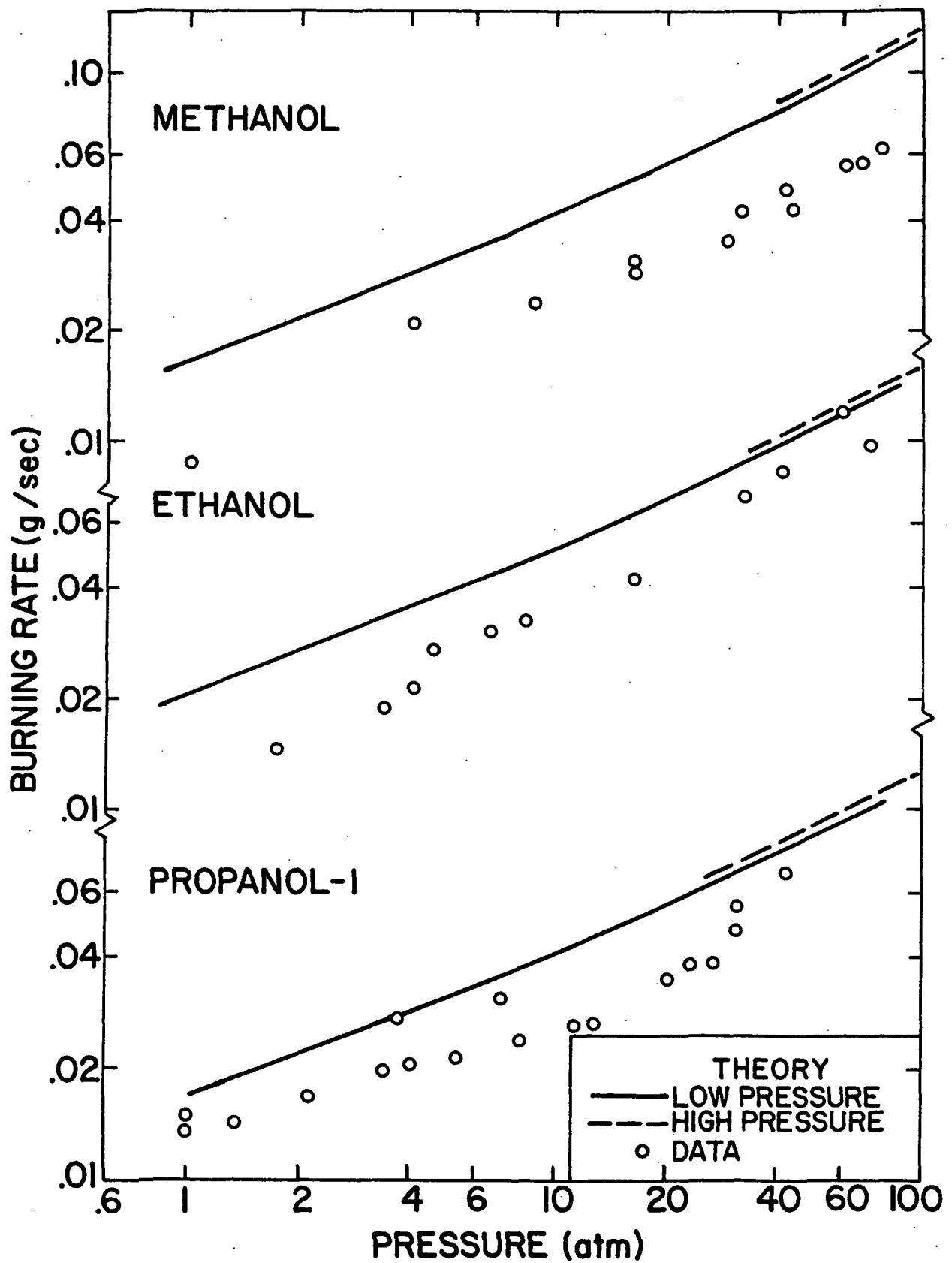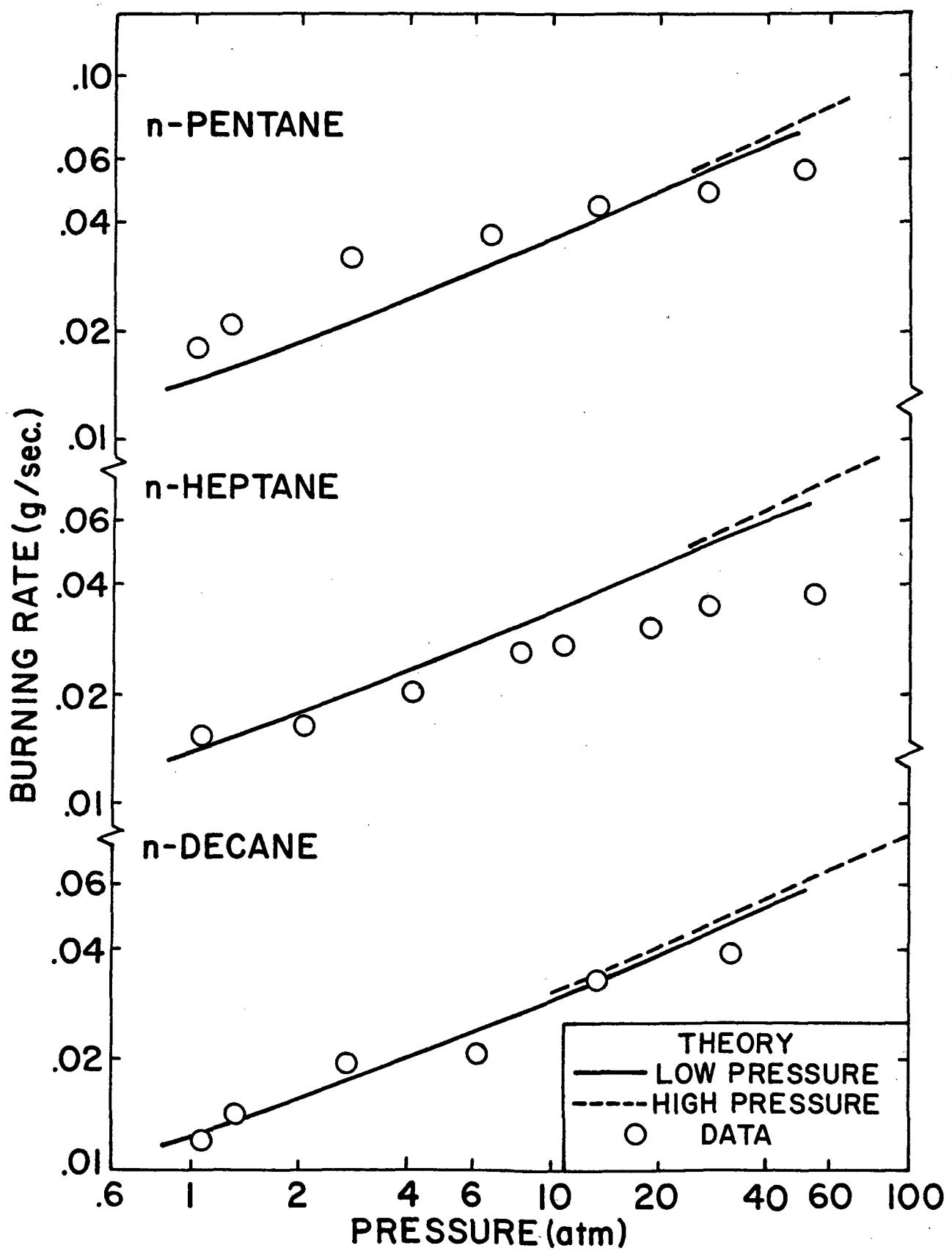
FIG. 4 EXPERIMENTAL BURNING RATES FOR HYDROCARBONS.
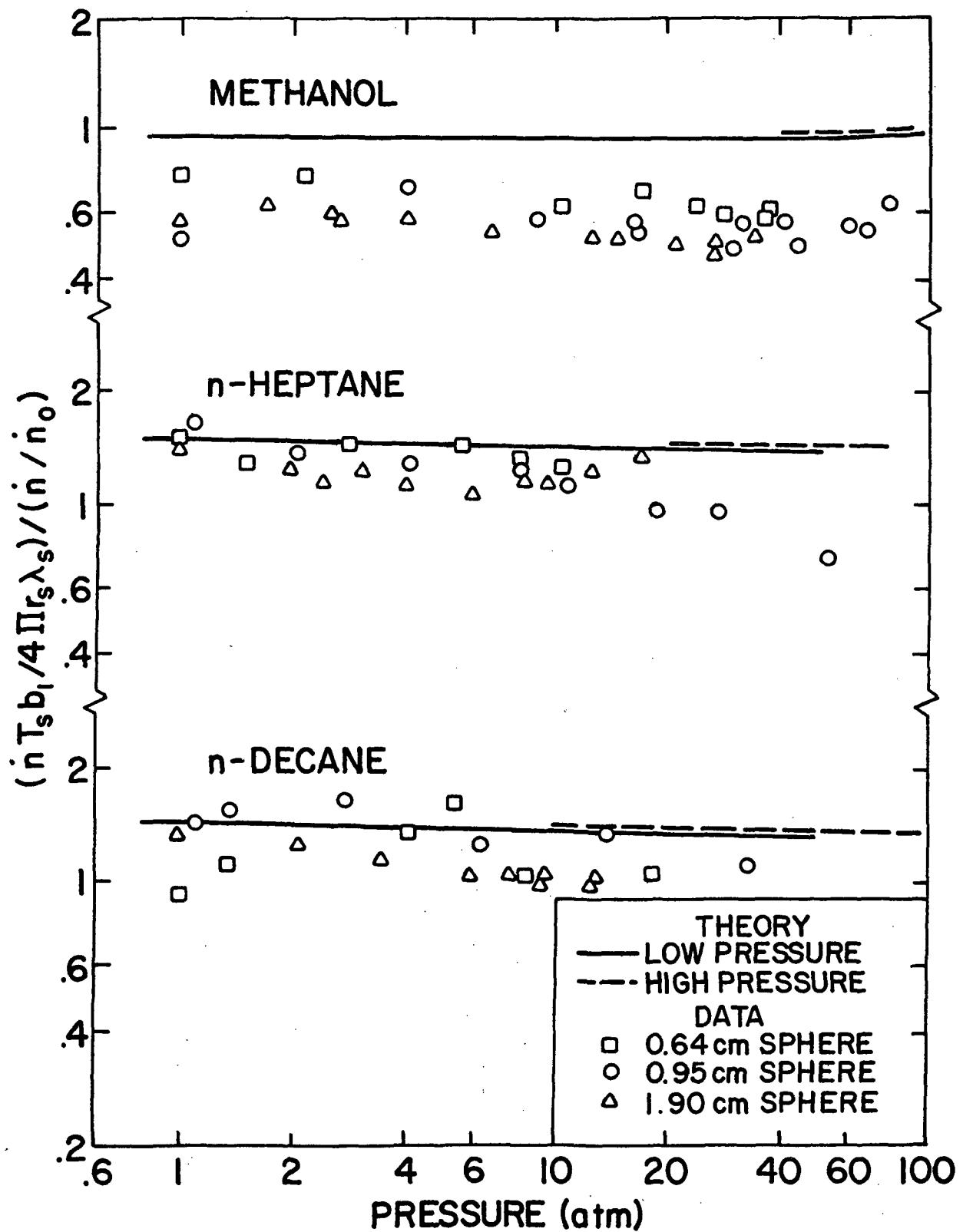
FIG. 5 BURNING RATES FOR VARIABLE SPHERE SIZES.

FIG. 6 LIQUID SURFACE TEMPERATURES FOR ALCOHOLS.

36

FIG. 7   LIQUID SURFACE TEMPERATURES FOR HYDROCARBONS.

37
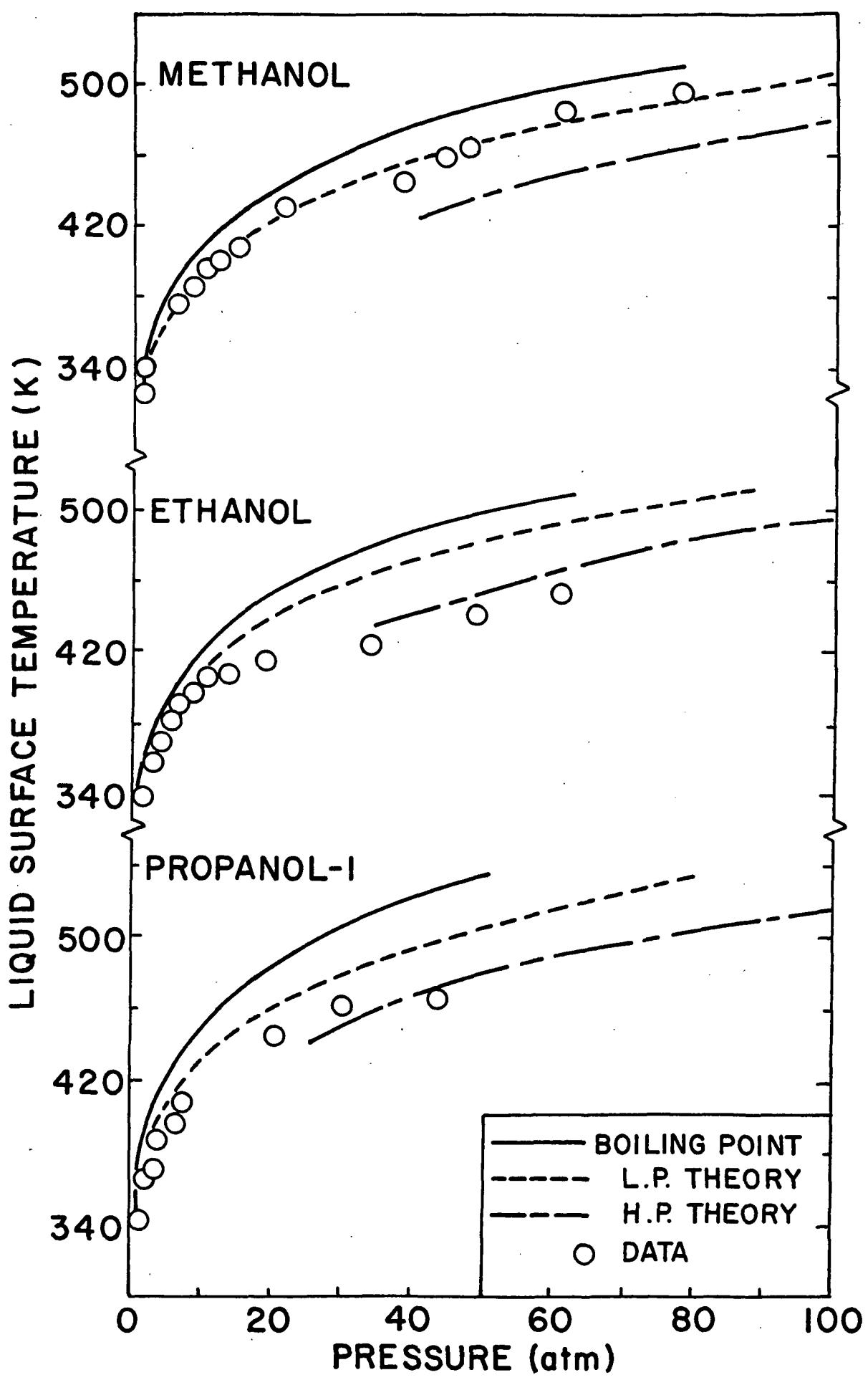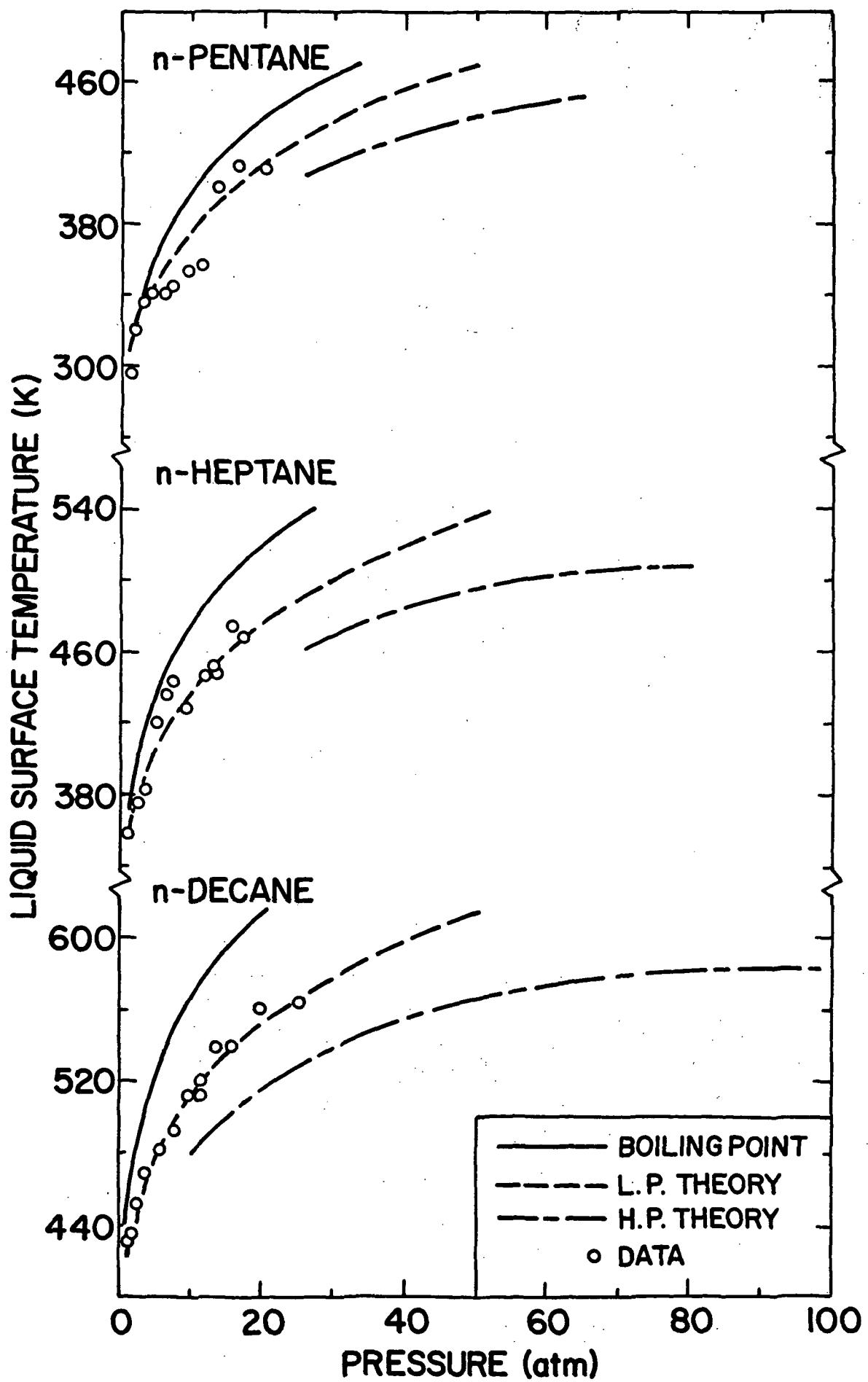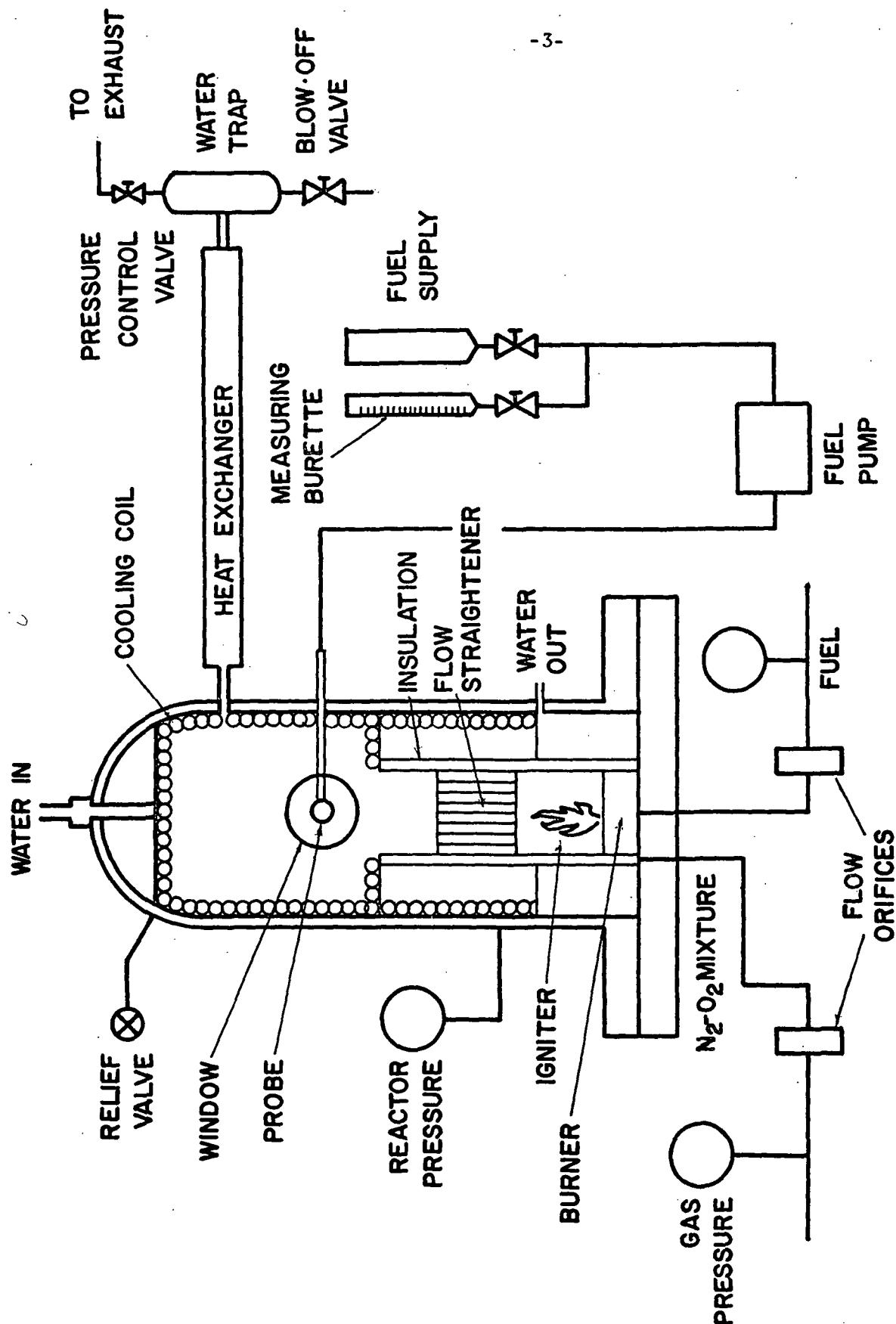
FIG. 8 HIGH PRESSURE COMBUSTION APPARATUS.
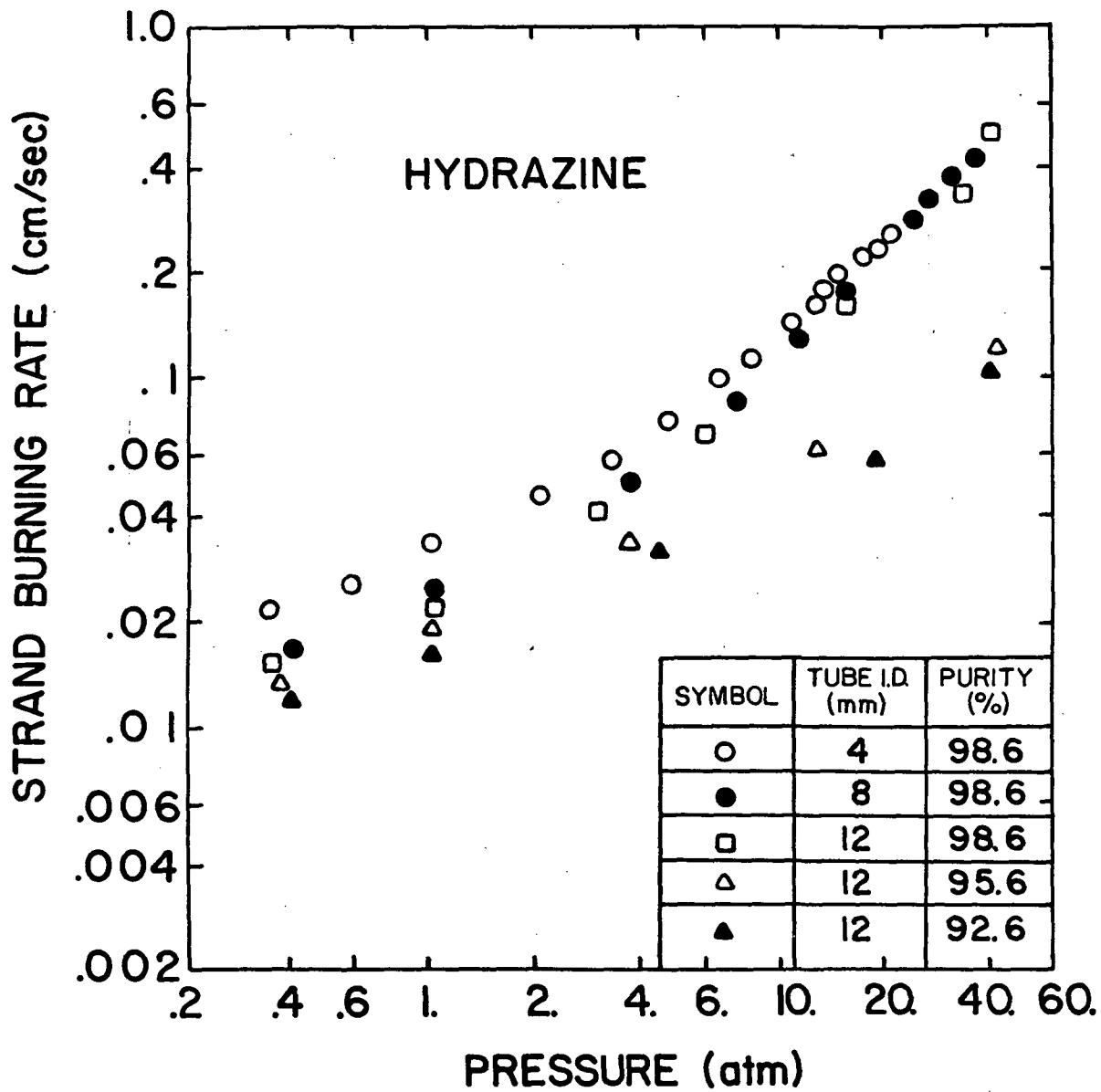
FIG. 9 HYDRAZINE STRAND BURNING RATES.

39
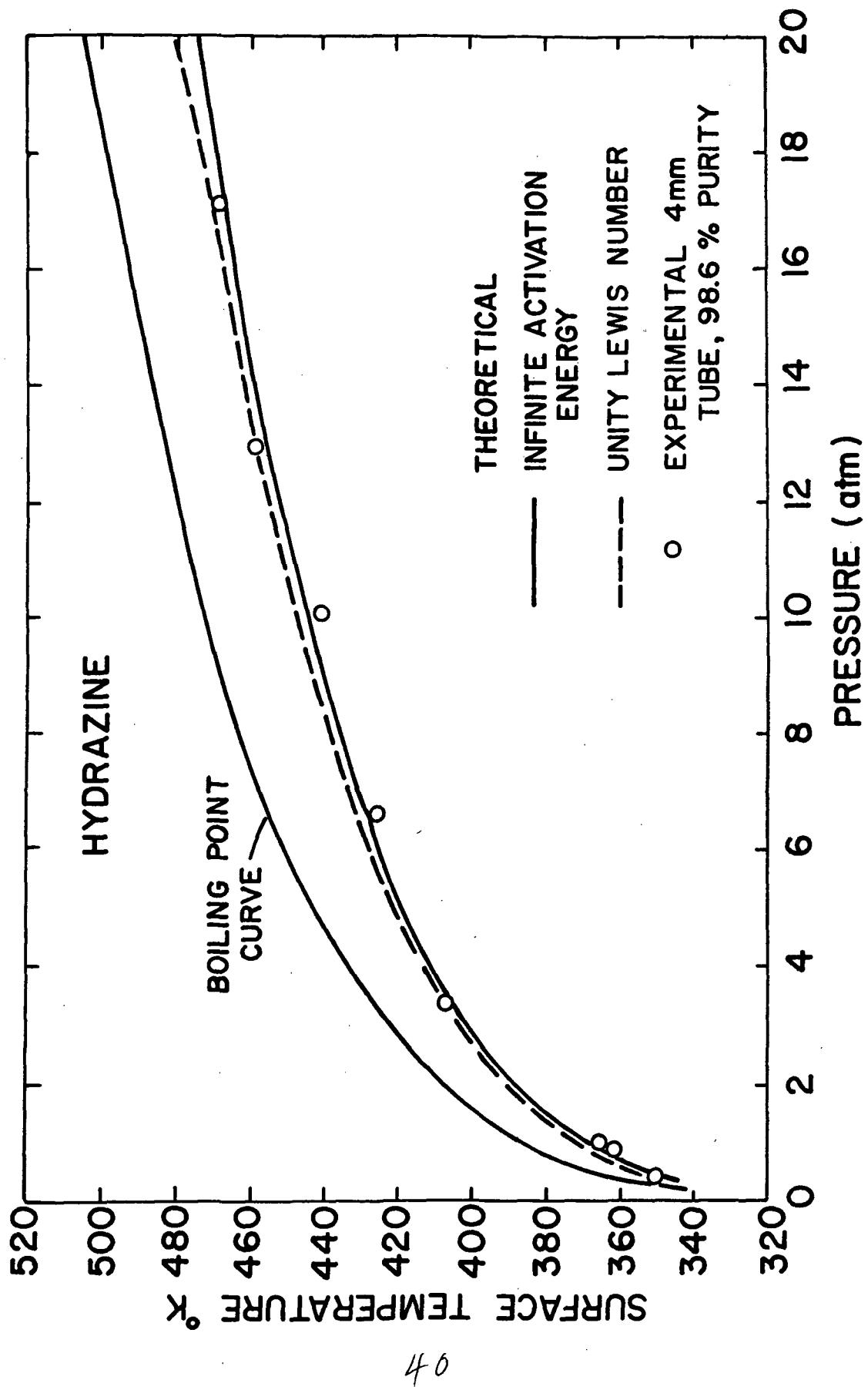
FIG. 10 LIQUID SURFACE TEMPERATURES DURING HYDRAZINE STRAND COMBUSTION.

40
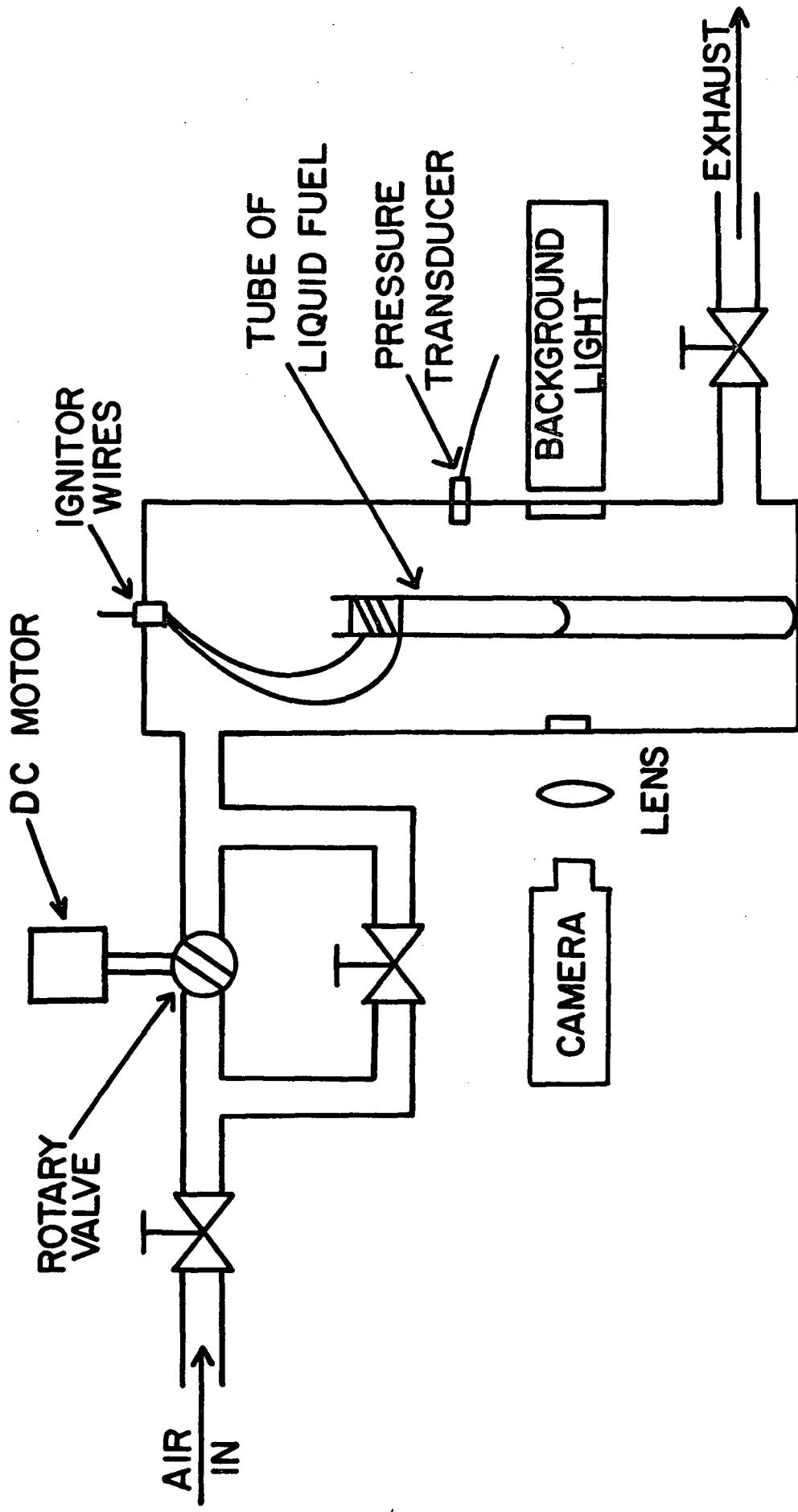
FIG. 11 SKETCH OF THE OSCILLATORY COMBUSTION APPARATUS.

41
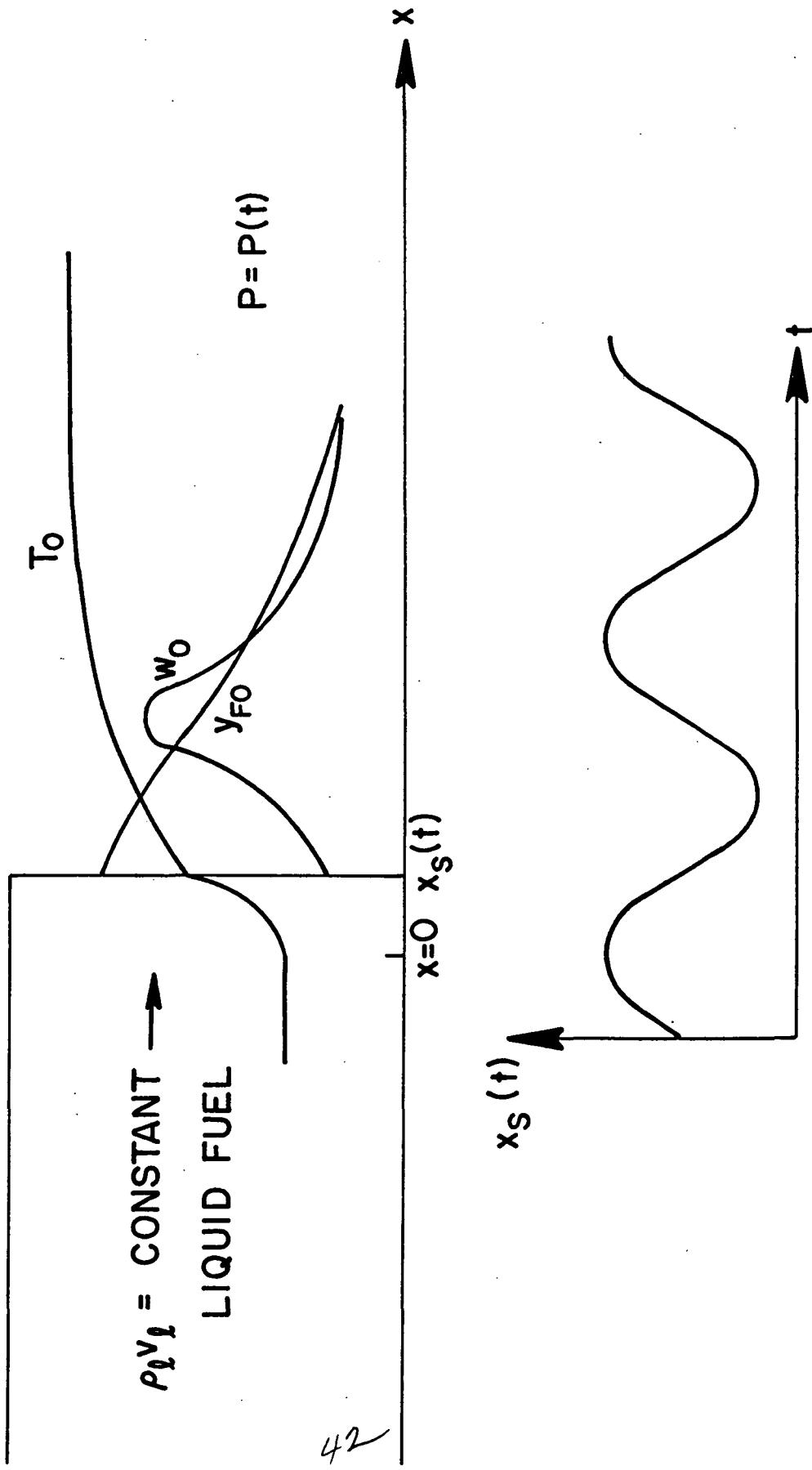
FIG. 12 SKETCH OF THE OSCILLATORY COMBUSION THEORETICAL MODEL.

42

1. Report No. 3 NASA CR-12111?	2. Government Accession No.	3. Recipient's Catalog No.
4. Title and Subtitle 1972 ANNUAL REPORT ON THE INVESTIGATION OF CRITICAL BURNING OF FUEL DROPLETS		5. Report Date January, 1972
		6. Performing Organization Code
7. Author(s) C. B. Allison, G. S. Canada, and G. M. Faeth		8. Performing Organization Report No.
		10. Work Unit No.
9. Performing Organization Name and Address Mechanical Engineering Department The Pennsylvania State University University Park, Pennsylvania 16802		11. Contract or Grant No. NGR 39-009-077
		13. Type of Report and Period Covered Contractor Report
12. Sponsoring Agency Name and Address National Aeronautics and Space Administration Washington, D. C. 20546		14. Sponsoring Agency Code

15. Supplementary Notes

Project Manager, Richard J. Priem, Chemical Propulsion Division,
NASA Lewis Research Center, Cleveland, Ohio

16. Abstract

Measurements of burning rate and surface temperatures were made for a number of liquid
alcohol and paraffin fuels from porous spheres in air under natural convection conditions.
The pressure levels of these experiments ranged up to 100 atm. Due to the high pressures,
theoretical models of this process included both low and high pressure versions, the latter
allowing for phenomena near the thermodynamic critical point of the liquid. The burning
rate predictions of the various theories were similar and found to be in fair agreement
with the data. Both theory and experiment indicated and approach to critical burning
conditions for methanol and ethanol at pressures in the range 80-100 atm. An experimental
apparatus was also constructed and testing is currently in progress on liquid fuel combustion
from porous spheres in a forced convection environment that simulates combustion chamber
conditions. Measurements have also been made of the liquid strand burning rates and surface
temperatures of hydrazine in the pressure range 7-600 psia. The burning rate was found to
increase linearly with pressure at pressures greater than atmospheric pressure. The
addition of small quantities of water to the hydrazine caused a marked reduction in the
burning rate at all pressures. Liquid surface temperatures were in good agreement with a
low pressure theory over the available test range. An apparatus has also been constructed
to study the response of a burning liquid hydrazine strand to imposed pressure oscillations
and testing with this apparatus is currently in progress. A theoretical model of this
oscillatory combustion process is presented with equations developed through first order in
the amplitude of the pressure oscillations.

7. Key Words (Suggested by Author(s)) Liquid fuel combustion High Pressure combustion Hydrazine fuel combustion Oscillatory combustion	18. Distribution Statement Unclassified - Unlimited	
9. Security Classif. (of this report) Unclassified	20. Security Classif. (of this page) Unclassified	21. No. of Pages 42	22. Price*